A spatial assessment of current and future foliar Hg uptake fluxes across European forests

Lena Wohlgemuth[1], Aryeh Feinberg[2], Allan Buras[3], and Martin Jiskra[4]

[1]Thünen Institut
[2]MIT
[3]Technical University of Munich
[4]Geosciences Environnement Toulouse, CNRS/OMP/Université de Toulouse

May 15, 2023

Abstract

Atmospheric mercury (Hg) is deposited to land surfaces mainly through vegetation uptake. Foliage stomatal gas exchange plays an important role for net vegetation Hg uptake, because foliage assimilates Hg via the stomata. Here, we use empirical relationships of foliar Hg uptake by forest tree species to produce a spatially highly resolved (1 km2) map of foliar Hg fluxes to European forests over one growing season. The modelled forest foliar Hg uptake flux is 23 ± 12 Mg Hg season-1, which agrees with previous estimates from literature. We spatially compare forest Hg fluxes with modelled fluxes of the chemistry-transport model GEOS-Chem and find a good overall agreement. For European pine forests, stomatal Hg uptake was shown to be sensitive to prevailing conditions of relatively high ambient water vapor pressure deficit (VPD). We tested a stomatal uptake model for the total pine needle Hg uptake flux during four previous growing seasons (1994, 2003, 2015/2017, 2018) and two climate change scenarios (RCP 4.5 and RCP 8.5). The resulting modelled total European pine needle Hg uptake fluxes are in a range of 8.0 - 9.3 Mg Hg season-1 (min - max). The lowest pine forest needle Hg uptake flux to Europe (8 Mg Hg season-1) among all investigated growing seasons is associated with unusually hot and dry ambient conditions in the European summer 2018, highlighting the sensitivity of the investigated flux to prolonged high VPD. We conclude, that stomatal modelling is particularly useful to investigate changes in Hg deposition in the context of extreme climate events.

https://www.overleaf.com/project/623c4a3b9809e1d1d1117124

A spatial assessment of current and future foliar Hg uptake fluxes across European forests

Lena Wohlgemuth[1,2], Aryeh Feinberg[3], Allan Buras[4], Martin Jiskra[1]

[1]Department of Environmental Geosciences, University of Basel, Basel, Switzerland
[2]Thünen Institute of Forest Ecosystems, Eberswalde, Germany
[3]Institute for Data, Systems, and Society, MIT, Cambridge, USA
[4]TUM School of Life Sciences, Technical University of Munich, Munich, Germany

Key Points:

- Extreme hot and dry atmospheric conditions have the potential to reduce stomatal uptake of ambient mercury by pine trees in Europe
- Atmospheric drought controls on stomatal mercury uptake should be accounted for in mercury transport models like GEOS-Chem
- Forest foliar mercury uptake fluxes to Europe from a bottom-up model generally agree well with results derived from literature and GEOS-Chem

Corresponding author: Lena Wohlgemuth, `lena.wohlgemuth@thuenen.de`

Abstract

Atmospheric mercury (Hg) is deposited to land surfaces mainly through vegetation uptake. Foliage stomatal gas exchange plays an important role for net vegetation Hg uptake, because foliage assimilates Hg via the stomata. Here, we use empirical relationships of foliar Hg uptake by forest tree species to produce a spatially highly resolved (1 km^2) map of foliar Hg fluxes to European forests over one growing season. The modelled forest foliar Hg uptake flux is 23 ± 12 Mg Hg $season^{-1}$, which agrees with previous estimates from literature.

We spatially compare forest Hg fluxes with modelled fluxes of the chemistry-transport model GEOS-Chem and find a good overall agreement. For European pine forests, stomatal Hg uptake was shown to be sensitive to prevailing conditions of relatively high ambient water vapor pressure deficit (VPD). We tested a stomatal uptake model for the total pine needle Hg uptake flux during four previous growing seasons (1994, 2003, 2015/2017, 2018) and two climate change scenarios (RCP 4.5 and RCP 8.5). The resulting modelled total European pine needle Hg uptake fluxes are in a range of 8.0 - 9.3 Mg Hg $season^{-1}$ (min - max). The lowest pine forest needle Hg uptake flux to Europe (8 Mg Hg $season^{-1}$) among all investigated growing seasons is associated with unusually hot and dry ambient conditions in the European summer 2018, highlighting the sensitivity of the investigated flux to prolonged high VPD. We conclude, that stomatal modelling is particularly useful to investigate changes in Hg deposition in the context of extreme climate events.

1 Introduction

Mercury (Hg) is a toxic pollutant that is transported globally through the atmosphere and deposited from air to land surfaces mainly through vegetation uptake of ambient gaseous elemental Hg(0) (Demers et al., 2013; Jiskra et al., 2015; Enrico et al., 2016; Obrist et al., 2017; Feinberg et al., 2022). Consequently, vegetation uptake has the potential to lower atmospheric Hg(0) transport and Hg deposition to oceans, where Hg can be methylated and bioaccumulated in marine seafood for human consumption (Zhou et al., 2021). In order to assess and improve the effectiveness of mitigation policies for human exposure, it is thus necessary to constrain environmental drivers of vegetation Hg(0) uptake. Furthermore, process understanding of vegetation Hg(0) uptake is essential for assessing future human Hg exposure in the context of global change (Sonke et al., 2023).

Global vegetation and soil uptake of Hg(0) has been estimated to amount to 2850 ± 500 Mg $year^{-1}$ (Obrist et al., 2021; Zhou et al., 2021; Feinberg et al., 2022), exceeding approximate direct anthropogenic emissions to the air of 2200 Mg Hg $year^{-1}$ (Sonke et al., 2023). Forests contain 80 % of the global plant biomass (Pan et al., 2013), therefore representing a major vector for Hg(0) drawdown from the atmosphere. In forests, half of the total Hg(0) net deposition is estimated to be stored in tree foliage, while the other half is estimated to be transferred to vascular tissues (e.g. stem, branches, roots), or taken up by understory vegetation (e.g. shrubs, grasses) or nonvascular plants (lichen and mosses) (Zhou et al., 2021; Obrist et al., 2021; Zhou & Obrist, 2021). In tree foliage, Hg concentrations increase linearly between foliage emergence and senescence (Rea et al., 2002; Laacouri et al., 2013; Blackwell et al., 2014; Wohlgemuth et al., 2020; Pleijel et al., 2021) implying a net foliar Hg deposition flux, albeit Hg re-emission from foliar surfaces of up to 30% of gross foliage Hg(0) deposition had been observed in a subtropical forest in China (W. Yuan, Sommar, et al., 2019). The bulk (90-96%) of Hg is stored in foliage tissues as opposed to leaf surfaces and correlates with leaf stomatal density (Laacouri et al., 2013). Studies on Hg stable isotopes in foliage (Demers et al., 2013; Zhou et al., 2021), enriched isotope tracer experiments (Rutter et al., 2011) and the vertical variation of net foliar Hg uptake in forest canopies (Wohlgemuth et al., 2020) strongly suggest a diffusive uptake pathway of atmospheric Hg(0) to foliage interiors via the stomata (Liu et al., 2021). In this way, foliar Hg(0) uptake is linked to foliage stomatal aperture for atmospheric gas exchange (Wohlgemuth et al., 2022).

Trees regulate foliage stomatal aperture to balance the inward diffusion of CO_2 for photosynthesis with the risk of desiccation caused by excessive outward diffusion of water vapor (Körner, 2013). The degree of stomatal aperture depends on atmospheric CO_2 levels and hydrological conditions (soil water availability and atmospheric evaporative demand) and varies among foliage-specific traits (age, tree species-specific evolutionary metabolic strategy and water use efficiency) (Körner, 2013). Pine, for instance, is an isohydric tree species capable of closing foliage stomata under warm and dry atmospheric conditions relatively early compared to tree species like oak and spruce (Lagergren & Lindroth, 2002; Zweifel et al., 2007, 2009), resulting in a reduced stomatal conductance for pine needle diffusive gas exchange (Panek & Goldstein, 2001). Consistently, Hg(0) uptake rates by pine needles in Europe were found to be lower at forest sites across Europe, where prolonged warm and dry atmospheric conditions prevailed over a given growing season during daytime (Wohlgemuth et al., 2022).

Species-specific stomatal response strategies to meteorological conditions are particularly relevant for projections of future foliar Hg uptake under climate change. Increasing global atmospheric temperatures driven by rising levels of greenhouse gases will result in an increased frequency of droughts (Grossiord et al., 2020) and higher soil moisture deficits (Berg & Sheffield, 2018; Stocker et al., 2019) in various regions of the world. These climatic conditions may decrease foliar Hg(0) uptake fluxes due to lower stomatal conductance (Wohlgemuth et al., 2022). A reduced plant Hg sink could further be amplified by deforestation and forest diebacks, particularly in the tropics (Allen et al., 2015; Brando et al., 2019; Feinberg et al., 2023). Other regions of the world are projected to become wetter through an increase in precipitation rates under climate change (IPCC, 2021a), which might lead to higher foliage stomatal conductance relative to the present and thus higher foliar Hg uptake. With continuing anthropogenic carbon emissions, an elevated atmospheric CO_2 level might have an antagonizing effect on the foliar stomatal Hg(0) uptake flux: foliar Hg(0) uptake could decline with decreasing stomatal conductance under CO_2 fertilization (Norby & Zak, 2011), or, the opposite, the vegetation sink for Hg(0) could increase with intensified biomass growth and higher soil C contents (Hararuk et al., 2013; Jiskra et al., 2018; H. Zhang et al., 2016). In order to make projections of the foliar Hg uptake flux in the next decades, these climate change impacts need to be further investigated and potentially implemented into global and regional Hg cycle models.

Current and future Hg fluxes are modelled in Global Chemical Transport Models (CTMs). CTMs like GEOS-Chem (Selin et al., 2008) apply resistance-based algorithms (Wesely, 2007) for modelling Hg(0) deposition fluxes from the atmosphere to vegetated ecosystems and are often based on parameters like leaf area indices (LAIs), temperature and wind speed. The resistance components for leaf stomata within CTMs commonly represent consensus values optimized to fit observations of Hg deposition velocities over vegetated surfaces (Selin et al., 2008; L. Zhang et al., 2009; Smith-Downey et al., 2010; H. Zhang et al., 2016), without taking stomatal feedback to environmental conditions into account (Wu et al., 2011; Khan et al., 2019). Consequently, forest tree species-specific stomatal responses to climate change at foliage level are not parameterized in CTMs. An additional problem related to CTMs is the uncertainty of modelled Hg(0) deposition fluxes due to insufficient model evaluation against dry deposition measurements (Feinberg et al., 2022). This issue of model validation was highlighted in a recent revision of GEOS-Chem parameterization after matching the GEOS-Chem model design to various experimental Hg(0) deposition measurements, which resulted in a doubling of the modelled global flux of Hg(0) dry deposition to land compared to previous model outcomes (Feinberg et al., 2022).

In this study, we assess the spatial variation of forest foliar Hg uptake fluxes across Europe by producing a spatially highly resolved map of foliar Hg uptake fluxes to European forests using a bottom-up model that incorporates pine tree stomatal responses to climate conditions. We compare these spatially resolved fluxes to forest dry deposition fluxes modelled in GEOS-Chem in order to identify spatial discrepancies between

GEOS-Chem and the bottom-up model used here. We investigate the sensitivity of an empirical stomatal response model of pine to different climatic conditions during past growing seasons and for two climate change projections of the years 2068 - 2082 in order to outline the potential of incorporating a stomatal response function into CTMs.

2 Materials and Methods

2.1 Description of datasets

For creating maps of foliar and pine needle Hg uptake fluxes in Europe applying a bottom-up model (Sect. 2.2 and 2.3), we drew on multiple data sources:

- **Foliar Hg data**. A dataset of foliar Hg uptake rates was derived from Hg measurements in foliage of tree canopies at 272 forest sites of the UNECE International Co-operative Programme on Assessment and Monitoring of Air Pollution Effects on Forests (ICP Forests). Forest sites are mostly located in Central and Northern Europe (+ 737 sites in Austria from the Austrian Bio-Indicator Grid) and harmonized foliage sampling methods were employed. All foliage samples within this dataset were harvested at the end of the growing seasons 2015 or 2017. Therefore, average foliage values of 2015/2017 constitute reference values of forest foliar Hg uptake fluxes relative to respective fluxes during investigated years of this study. The dataset is publicly available and contains 3569 foliar Hg concentrations of 23 tree species and is described in detail in (Wohlgemuth et al., 2022).
- **Meteorological data**. Values on ambient temperature and relative humidity at surface air pressure (1000 hPa) in Europe (spatial resolution: 0.25° x 0.25°) originate from ERA5 hourly reanalysis data and were downloaded from the Copernicus Climate Data Store (Hersbach et al., 2018). The applied time frame includes hourly daytime (07:00 - 18:00 LT) values during the respective growing seasons (April - October) of 1994, 2003, 2015, 2017, and 2018.
- **Climate change data**. Regional climate simulation data of air temperature and relative humidity at 2 m above surface level for the years 2068 - 2082 and two different climate change scenarios (Representative Concentration Pathway (RCP) 4.5 and RCP 8.5 (IPCC, 2021b)) were obtained from the Coordinated Regional Climate Downscaling Experiment (CORDEX) (Jacob et al., 2020) framework for the European domain with a spatial resolution of 0.11° x 0.11° and a temporal resolution of 3hourly daytime (09:00 - 18:00 LT) values. For representing a range of different climate model outputs, we calculated average values from multiple regional climate models (RCMs) downscaled from global climate models (GCMs) depending on availability for download from the Copernicus Climate Data Store (C3S, 2022). In total, we incorporated data of 15 combinations of 4 RCMs and 6 GCMs for RCP 4.5 and of 13 combinations of 6 RCMs and 8 GCMs for RCP 8.5 (see Table SI 3) for an overview of models and ensemble members).
- **European tree species distribution**. We used a map of spatial proportions of tree species groups per km^2 land area from (Brus et al., 2012). For use in calculating pine foliar Hg uptake fluxes (see Sect. 2.3), we summed up spatial relative abundance values of *Pinus sylvestris*, *Pinus pinaster*, *Pinus nigra* and *Pinus halepensis* from European forest inventories (Mauri et al., 2017; Buras & Menzel, 2019) and multiplied these pine relative abundances with the respective total forest area per km^2 derived from (Brus et al., 2012) to obtain pine areal proportions. We performed the same calculation (sum of values of *Pinus sylvestris*, *Pinus pinaster*, *Pinus nigra* and *Pinus halepensis* and subsequent multiplication with respective total forest area) to estimate the distribution of pine in Europe under climate change using relative abundance probabilities projected from climate analogues for the time period 2061 - 2090 and RCP 4.5 and RCP 8.5 by (Buras & Menzel, 2019).

- **Leaf Area Indices (LAIs) and Leaf Mass per Area (LMA) values**. We used the LAI satellite product (spatial resolution: 330 m) of PROBA-V (Dierckx et al., 2014; Fuster et al., 2020) to upscale foliar Hg uptake rates at each ICP Forests site to foliar Hg uptake fluxes (see Sect. 2.2), along with average LMA values per tree species from (Forrester et al., 2017).

2.2 Calculation of forest foliage Hg uptake fluxes

We determined forest foliar Hg uptake fluxes to European forests on a 1 km^2 spatial resolution applying three basic computational steps: 1) calculation of tree species-specific daily Hg uptake fluxes per m^2 ground area using a bottom-up model; 2) upscaling of respective foliar Hg fluxes per tree species to the European forested area using the areal distribution of corresponding tree species; 3) multiplication of daily forest foliar Hg uptake fluxes per latitude with latitude-dependent growing season length in order to obtain the forest foliar Hg uptake fluxes over one growing season.

Computational step 1) is based on the premise, that foliar Hg uptake rates are tree species-specific (Laacouri et al., 2013; Wohlgemuth et al., 2022; Pleijel et al., 2021). For this reason, we calculated median daily foliar Hg uptake fluxes per tree species group (see Table SI 2 for details) of all forest sites from the foliar Hg dataset (Sect. 2.1). The bottom-up modeling approach for calculating daily foliar Hg uptake fluxes from daily foliar Hg uptake rates is described in detail in Wohlgemuth et al., (2020) (Wohlgemuth et al., 2020). Briefly, daily foliar Hg uptake rates per gram foliage dry weight (units of ng Hg $g_{d.w.}^{-1}$ d^{-1}) were multiplied with tree species-specific LMA values (Sect. 2.1) to obtain daily foliar Hg uptake rates per foliage surface area (ng Hg m_{leaf}^{-2} d^{-1}). Subsequently, values of daily foliar Hg uptake rates per foliage surface area are multiplied with values of LAI (m_{leaf}^{2} m_{ground}^{-2}; Sect. 2.1), resulting in daily foliar Hg fluxes per unit ground area (ng Hg m_{ground}^{-2} d^{-1}). LAI values of coniferous forests are relatively constant during the active growing season after the initial growth phase of current-season needles (R. Wang et al., 2017), while LAI values of temperate deciduous forests increase rapidly at the beginning of the growing season (leaf flushing) and climax at peak season (June – August, northern hemisphere) (Q. Wang et al., 2005). For coniferous tree species, we used the maximum LAI value during the constant period at each forest site of the ICP Forests dataset to calculate needle foliar Hg uptake fluxes. For deciduous tree species, we calculated foliar Hg uptake fluxes as a temporal sequence at every LAI value available over the growing season and subsequently used median foliar Hg uptake flux values of the growing season. For LAI values larger than 3, we applied a species-specific tree height correction factor, to account for lower foliar Hg uptake fluxes of shaded leaves in the lower canopy (Wohlgemuth et al., 2020) (refer to Table SI 1 for utilized tree height correction factors). For coniferous species, we multiplied Hg uptake fluxes of current-season needles with a species-specific needle age correction factor to account for lower Hg uptake rates of older needle age classes (Wohlgemuth et al., 2020) (refer to Table SI 1 for utilized needle age correction factors).

Computational step 2) involves the multiplication of the proportion of each tree species per km^2 land area with the respective species-specific median daily foliar Hg uptake fluxes. We matched tree species-specific Hg data with the areal forest distribution of the respective tree species (Brus et al., 2012). In the few cases of rare European tree species, where specific Hg data was lacking, we pooled Hg or forest distribution data by tree species group (see Table SI 2 for an overview of matched tree species groups between the two datasets). Subsequently, we added up all tree species-specific daily foliar Hg uptake fluxes within each km^2 and obtained one forest foliar daily Hg uptake flux per km^2.

In computational step 3) we calculated forest foliar Hg uptake fluxes per km^2 and one growing season by multiplying each daily foliar Hg uptake flux per km^2 with the growing season length in days following a simple latitudinal model (CLRTAP, 2017). The latitudinal model of growing season determines a growing season length of 192 days at latitude 50° and decreases by 3.5 days per 1° of latitude moving north and increases by 3.5 days per 1° of latitude moving south.

2.3 Calculation of pine foliar Hg uptake fluxes

Daily foliar Hg uptake rates of pine tree species were calculated taking into account the empirical dependence of needle Hg uptake fluxes to atmospheric VPD. Pine needle daily Hg uptake rates (upR_{pine}; ng Hg $g_{d.w.}^{-1}$ d^{-1}) were found to be lower at forest sites, where the daytime fraction of water VPD > 1.2 kPa during the respective sample life period ($proportion_{dayVPD} > 1.2$kPa) was relatively high (Wohlgemuth et al., 2022). The negative correlation of pine needle Hg uptake with timespan of elevated atmospheric VPD was explained by a stomatal closure upon VPD threshold exceedance and thus a high stomatal resistance suppressing the diffusive uptake of Hg(0) from the atmosphere. The linear regression of daily foliar Hg uptake rates with $proportion_{dayVPD} > 1.2$ kPa is: upR_{pine} = 0.116 – 0.13 x ($proportion_{dayVPD} > 1.2$ kPa) (Wohlgemuth et al., 2022). We applied this linear relationship to calculate the pine foliar Hg uptake rates of the forest area of Europe during four different growing seasons in 1994, 2003, an average of 2015 and 2017, 2018, and projected for the time period 2068 - 2082 under RCP 4.5 and RCP 8.5 (IPCC, 2021b). We calculated hourly or 3hourly daytime VPD values from ERA5 (Hersbach et al., 2018) or CORDEX data (Sect. 2.1) on surface temperature and relative humidity using the Auguste-Roche-Magnus formula (W. Yuan, Zheng, et al., 2019) and subsequently determining the fraction of daytime hours when the VPD was above the threshold of 1.2 kPa over the respective latitudinal growing season length. Calculations with climate data were performed at sciCORE scientific computing center at University of Basel. We defined growing season length per latitude using a latitudinal model ((CLRTAP, 2017), see Sect. 2.2). In 2068 - 2082 we assumed the beginning of the growing season to be 3 days earlier and the end of the growing season to be 3 days later to take increases in growing season length under climate change into account (Jeong et al., 2011; Garonna et al., 2014). The underlying areal distribution of pine is based on European forest inventories and projections of pine abundances based on climate analogues under RCP 4.5 and RCP 8.5 by (Buras & Menzel, 2019) (see Sect. 2.1).

2.4 GEOS-Chem forest deposition flux calculation

GEOS-Chem is a global 3-D chemistry transport model, which includes a comprehensive Hg cycle (Selin et al., 2008). Table 1 gives an overview of the methodological approach and input parameters for calculating the respective Hg fluxes of GEOS-Chem and the bottom-up model (Sect. 2.2), which we compared spatially in this study.

Table 1. Caption

	bottom-up model	**GEOS-Chem**
model input parameters	spatial forest distribution (Brus et al., 2012); leaf area indices (LAIs) (Dierckx et al., 2014; Fuster et al., 2020); leaf mass per area (LMA) (Forrester et al., 2017); meteorological parameter: daytime VPD (Hersbach et al., 2018); foliar Hg uptake rates (Wohlgemuth et al., 2022)	spatial forest distribution (Gibbs, 2006); leaf area indices (LAIs) (H. Yuan et al., 2011); atmospheric Hg(0) levels (GEOS-Chem v12.8.1 simulation 2015); meteorological parameters: air temperature, pressure, solar radiation, cloud cover, wind speed (GEOS-FP) (Lucchesi, 2018)
spatial resolution	1 km x 1 km	0.25 x 0.3125°
basic methodological approach for Hg flux calculation	spatial upscaling of measured foliar Hg uptake rates (Wohlgemuth et al., 2020)	in-series calculation of Hg dry deposition velocity from parameterized resistance values (Wesely, 2007)
foliage stomatal Hg uptake flux component	calculated for pine based on daytime vapor pressure deficit (VPD) values (Sect. 2.3)	calculated within the canopy resistance component as a function of land type, leaf area indices (LAIs), and solar radiation
model output compared in this study	tree-species specific forest foliar Hg(0) uptake fluxes	Hg(0) dry deposition fluxes to coniferous and deciduous forest land cover

We used an offline version of the GEOS-Chem dry deposition code (Feinberg, 2022) to be able to calculate dry deposition velocities at higher resolution and only for certain land use types (i.e., forest areas). The offline dry deposition code computes deposition velocities using a resistance-based approach (Y. Wang et al., 1998; Wesely, 2007). Input variables (Table 1) are gridded hourly GEOS-FP meteorological data for (e.g., air temperature, wind speed, solar radiation, and cloud cover) and weekly LAI values based on MODIS (H. Yuan et al., 2011) for the year 2015. The model calculates the Hg(0) dry deposition velocity based on species-specific parameters including its biological reactivity ($f_0 = 10^{-5}$) and Henry's Law Constant ($H^* = 0.11$ M atm^{-1}). To isolate the uptake of Hg(0) to forests, we calculated the dry deposition velocity only over coniferous and deciduous land cover types from the Olson land map (Gibbs, 2006). The offline calculations output hourly dry deposition velocities over the European domain at $0.25 \times 0.3125°$ resolution. We converted the calculated Hg(0) deposition velocities to fluxes by multiplying with hourly surface Hg(0) concentrations from a GEOS-Chem v12.8.1 simulation for 2015. For this study, we compared the GEOS-Chem Hg(0) dry deposition fluxes to forests with foliar Hg(0) uptake fluxes calculated using the bottom-up model. For both models, Hg fluxes were averaged over the latitude-dependent growing season length in days and cropped to the same spatial extent. As GEOS-Chem and the bottom-up model differ in their geographic resolution (GEOS-Chem: 0.25° x 0.31° $\sim$ 955 km^2 vs. bottom-up: 1 km^2), we downsampled daily forest foliar Hg uptake fluxes from the bottom-up model through bilinear interpolation.

2.5 Uncertainty analysis of foliar Hg uptake fluxes

The relative uncertainty value per tree species group depended on propagated uncertainties of calculation parameters used to derive the respective foliar Hg uptake flux per tree species group (see Table SI 4 for details and values). Subsequently, we calculated one relative uncertainty value per geographic tile of our European flux map (Fig. 1) by summarizing the relative uncertainty of each foliar Hg uptake flux per tree species group within each tile according to error propagation principles (Ku, 1966; Papula, 2003). We obtained the relative uncertainty for the total foliar Hg uptake flux to European forests (Fig. 1) by propagating all relative uncertainty values per tile. The final relative uncertainty value of total foliar Hg uptake flux to European forests and the reference growing seasons 2015/2017 is 0.52.

3 Results and Discussion

3.1 Spatial distribution of forest foliar Hg uptake fluxes across Europe

Figure 1 visualizes forest foliar Hg uptake fluxes per growing season at a spatial resolution of 1 km^2 (g Hg km^{-2} season^{-1}) in Europe. Forest foliar Hg uptake fluxes generally follow a spatial distribution of European forests, because this map (Fig. 1) is based on the proportion of forest tree species per land area (Brus et al., 2012). Consequently, the largest forest foliage Hg uptake fluxes in terms of area are on the Scandinavian Peninsula with dense forest land cover. Outside of Scandinavia, forest foliage Hg uptake fluxes fall along large contiguous forested areas, e.g. in the Carpathian Mountains, the South-Eastern Alps, the Balkans, or forested low mountain areas like the Black Forest.

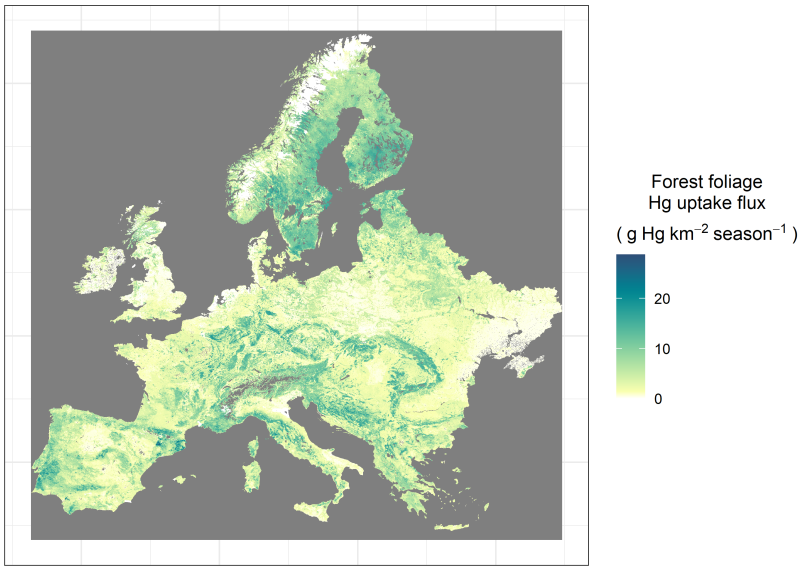

Figure 1. Spatial distribution of forest foliar Hg uptake fluxes (g Hg km^2 growing season^{-1}) to Europe based on a bottom-up extrapolation of foliar Hg concentrations, that were measured and averaged over the 2015 and 2017 growing seasons. Dark grey areas represent excluded non-forested areas (e.g. surface waters or non-vegetated mountain areas).

The sum of forest foliar Hg uptake fluxes over the land area of Europe as displayed in Figure 1 equals 23 ± 12 Mg Hg season^{-1}. This total flux agrees within uncertainty

with a previous estimate for the total foliar Hg uptake flux to Europe of 20 ± 3 Mg Hg over the 2018 growing season based on foliar Hg uptake fluxes at four forested sites (Wohlgemuth et al., 2020). (Zhou & Obrist, 2021) evaluated a median global foliar Hg assimilation of 28 Mg yr^{-1} for deciduous broadleaf forests and 61 Mg yr^{-1} for evergreen needleleaf forests by combining foliar Hg concentrations with annual net foliar biomass production data of the respective forest types. From these global assimilation estimates by (Zhou & Obrist, 2021), we calculated a total foliar Hg assimilation of 29 Mg yr^{-1} to the deciduous and coniferous forest land area of Europe (for details see SI, Text S1), which is slightly higher but still within the uncertainty of the 23 ± 12 Mg Hg $season^{-1}$ from this study. However, foliar Hg uptake fluxes based on net primary foliar biomass production by Zhou and Obrist, (2021) (Zhou & Obrist, 2021) does not correct for lower foliar Hg uptake rates by shade leaves and multiyear old needles (see Sect. 2.2) relative to sun leaves and younger needles (Wohlgemuth et al., 2020), likely resulting in a systematic over-estimation. We assume, that the different time reference (seasonal vs. annual) of the flux from this study (23 ± 12 Mg Hg $season^{-1}$) and the flux derived from Zhou and Obrist, (2021) (Zhou & Obrist, 2021) (29 Mg Hg yr^{-1}) only plays a minor role for explaining the difference between the two fluxes, since we expect a small net foliar biomass production in Europe in winter outside of the growing season.

3.2 Pine foliar Hg uptake fluxes under different VPD scenarios

Figure 2 shows total pine forest foliar Hg uptake fluxes to Europe calculated under different conditions of atmospheric surface-level water VPD during four past growing seasons (1994, 2003, 2015/2017, 2018) and simulated for the years 2068 - 2082 as an average of multiple climate model outputs (see Sect. 2.2) under two different climate change scenarios (RCP 4.5 and RCP 8.5). The leftmost bar (Fig. 2) represents a theoretical baseline pine needle Hg uptake flux in absence of VPD induced stomatal control (potential maximum transpiration rates) on the pine needle Hg uptake flux. The total pine needle Hg uptake flux to Europe during the reference growing season 2015/2017 (Sect. 2.2) is 9.3 ± 3.7 Mg Hg representing 70% of the baseline flux of 13.3 ± 5.3 Mg Hg $season^{-1}$. Thus, based on the pine needle Hg uptake model used in this study (Sect. 2.3), the VPD effect reduces the total pine needle Hg uptake flux to Europe by approximately 30%.

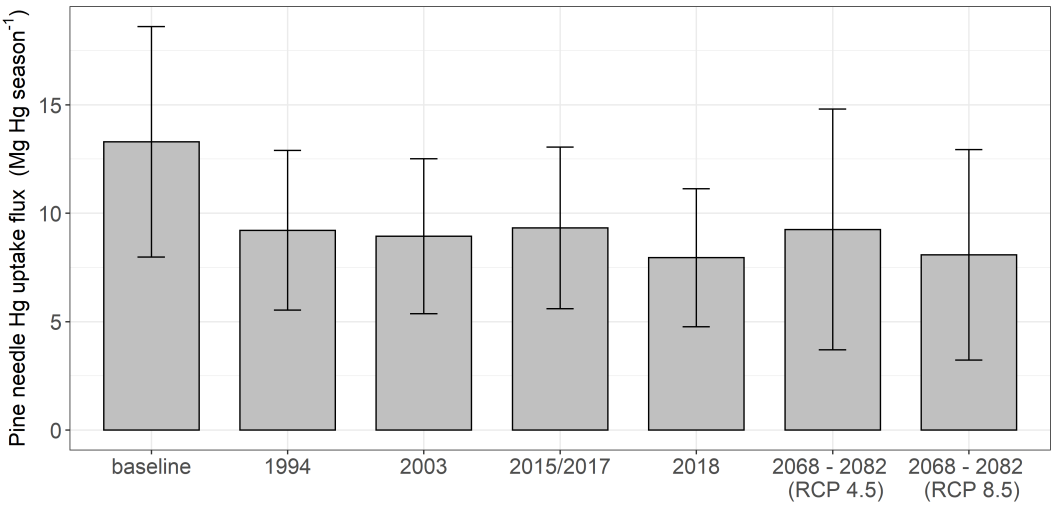

Figure 2. Pine needle Hg uptake flux to European pine forests (Mg Hg season^{-1}) calculated from atmospheric surface water vapor pressure deficit (VPD) conditions during the growing seasons 1994, 2003, 2015/2017, 2018 and projected for the years 2068 - 2082 under RCP 4.5 and RCP 8.5. Bar on the left represents a baseline pine forest needle Hg uptake flux with no VPD exceedance of 1.2 kPa throughout the growing season.

The relative standard deviation of modelled total pine needle Hg uptake fluxes for the investigated growing seasons (1994, 2003, 2015/2017, 2018, 2068 - 2082) was 0.07. Consequently, modelled total European pine needle Hg uptake fluxes hardly differed from each other among growing seasons. The total pine needle Hg uptake flux in Europe depend on VPD conditions in areas where pine forests prevail. Pine forests are primarily located in Northern Europe (SI Fig. 1), where hourly ambient VPD was > 1.2 kPa during 30% or less of daytime in the growing seasons 1994, 2003 and 2015/2017 due to relatively cool and moist ambient conditions as compared to Central and Southern Europe (see e.g. VPD conditions during reference time period 2015/2017 Fig. 3a). In contrast to previous years, the European summer hydrological condition of 2018 has been described as an intense hot drought, during which pronounced stomatal closure of coniferous forests in response to high VPD were recorded in Switzerland (Gharun et al., 2020). In Southern Fennoscandia, conditions of ambient hourly VPD > 1.2 kPa prevailed over exceptionally long time proportions (around 40%) during the summer of 2018 (see Fig. 3b, (Buras et al., 2020)). As a result, the modelled total pine needle Hg uptake flux in Europe in 2015/2017 (9.3 Mg Hg season^{-1}) was by a factor of 1.16 higher than the respective flux in 2018 (8.0 Mg Hg season^{-1}). We conclude that hot and dry summer conditions (Fig. 2) in Fennoscandia crucially impact modelled past total pine needle Hg uptake fluxes in Europe. According to the model results, an average amount of 1.3 Mg Hg was not deposited via pine needle uptake in 2018 compared to 2015/17, potentially remaining in the atmosphere, where it can be long-range transported to the ocean (Zhou et al., 2021). These 1.3 Mg Hg are more than three times larger than the reported anthropogenic Hg emissions of Sweden in 2021 **??**, highlighting the quantitative impact, that hot droughts can have on the pine needle Hg uptake flux.

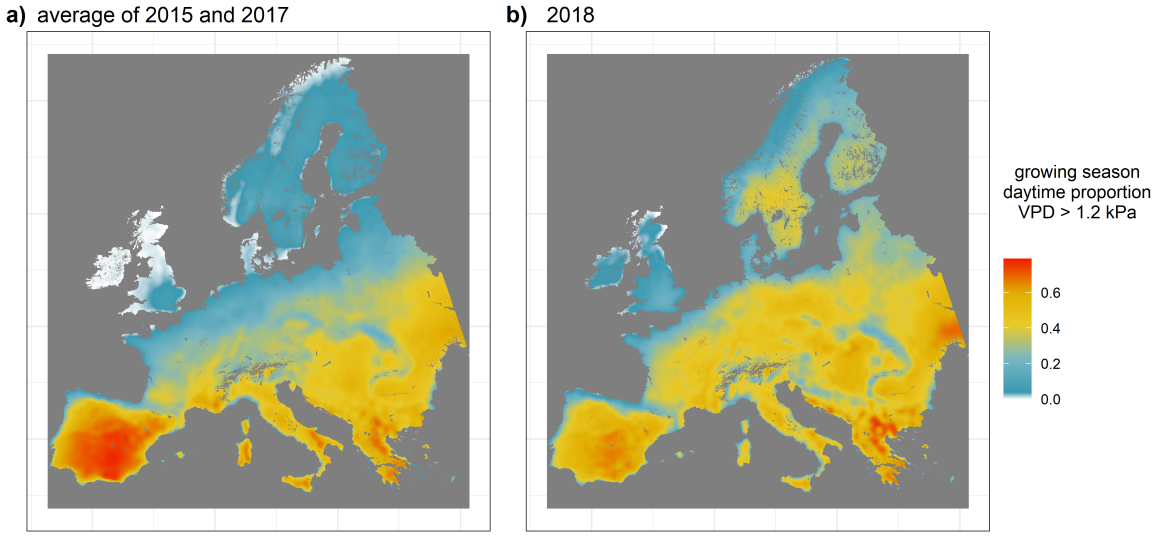

Figure 3. Average daytime proportion of surface level atmospheric water VPD > 1.2 kPa during a) the reference growing season 2015/2017, and b) the growing season 2018. All VPD values were calculated from hourly reanalysis data of ERA5 ambient air temperature and relative humidity (Sect. 2.1).

3.3 Projected pine forest needle Hg uptake fluxes under climate change scenarios

The projected total pine forest needle Hg uptake flux for 2068 - 2082 (RCP 4.5: 9.3 ± 5.5 Mg Hg season^{-1}; RCP 8.5: 8.1 ± 4.9 Mg Hg season^{-1}) was in the same range as the corresponding average flux for the years 1994, 2003, 2015 and 2017 of 9.1 ± 0.2 Mg Hg season^{-1} (mean ± sd), but slightly higher than the corresponding flux in the year of 2018 (8.0 ± 3.2 Mg Hg season^{-1}), during which Fennoscandia experienced a summer of relatively long hot and dry ambient conditions. Figure 4 maps the absolute deviation of the pine forest needle Hg uptake flux projected for 2068 - 2082 (simulated future flux) from the corresponding 2018 flux in Europe. Under RCP 4.5, the simulated future flux is higher (blue area in Fig. 4 a) than the 2018 flux in 65% of total area. Under RCP 8.5, the simulated future flux is higher (blue area in Fig. 4 b) than the 2018 flux in 43% of total area. In most area of Fennoscandia, where a majority of pine forests in Europe are located (SI Fig. 1a), the future flux is projected to be larger than in 2018. For both climate change scenarios, the projection predicts lower pine needle Hg fluxes to the Balkans and to the Southern Iberian Peninsula than in 2018 (Fig. 4).

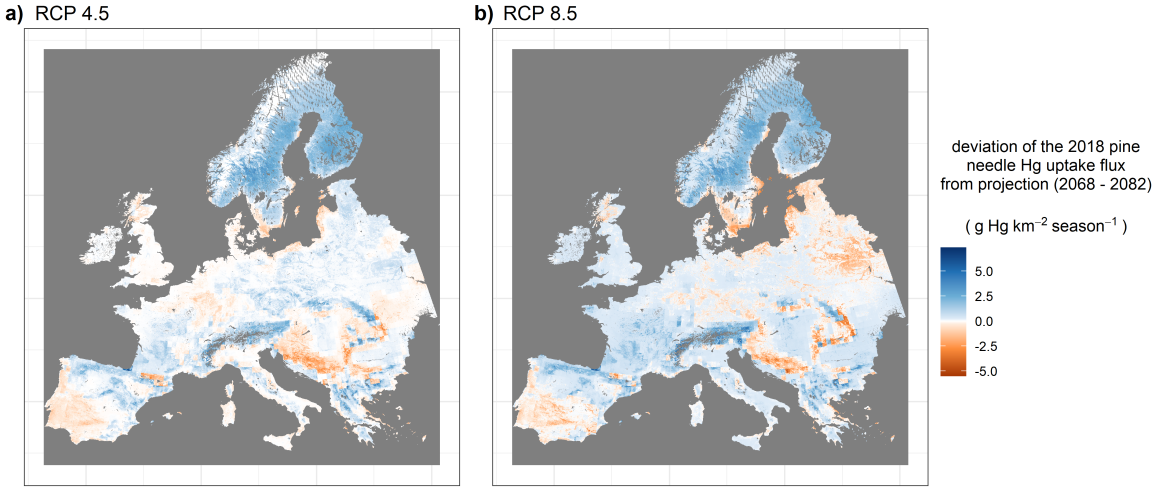

Figure 4. Absolute deviation of projected pine forest foliar Hg uptake fluxes for 2068 - 2082 (under RCP 4.5 (a) and RCP 8.5 (b)) from the corresponding flux modelled for 2018. In blue areas, the projected future flux under the two climate change scenarios is higher than the respective 2018 flux, in orange areas, this deviation is reversed.

The pine forest needle Hg uptake flux for 2068 - 2082 simulated here is a function of both modelled ambient VPD conditions during the growing season and the projected distribution of pine forests in Europe depending on climate analogs (Buras & Menzel, 2019). While the pine forest cover in Southern Sweden is projected to decrease under the climate change scenarios RCP 4.5 and RCP 8.5 from around 50% km^{-2} to around 25% km^{-2}, forest cover in Central and Northern Fennoscandia is projected to be relatively steady for climate analogs of both climate change scenarios (compare SI Fig. 1 a - c). Average long-term precipitation rates are projected to increase in Scandinavia, along with a decrease of meteorological drought in the coming decades under different climate change scenarios (Forzieri et al., 2014; Samaniego et al., 2018; Kellomäki et al., 2018), which could result in an increase of atmospheric humidity and a decrease of VPD in northern Europe (Oksanen et al., 2019). Under this scenario of wetter forest environments, the Hg sink of Scandinavian pine forest needles would not be significantly diminished. However, drought trends in Fennoscandia are still inconsistent and extreme drought events like in 2018 might occur more frequently under the current rate of climate change (IPCC, 2021a). The summer of 2018 was a record hot drought in Europe (Buras et al., 2020), while climate simulations for 2068 - 2082 are averaged over multiple climate models (SI Table 3), possibly averaging out extreme events. In a scenario, where the maximum proportion of daytime VPD $>$ 1.2 kPA per growing season averaged over 2068 - 2082 prevails at each spatial unit, the total pine forest needle Hg uptake flux to Europe reduces to 6.9 Mg Hg season^{-1} for RCP 4.5 and 5.0 Mg Hg season^{-1} for RCP 8.5, which corresponds to 74% and 62% of the respective flux derived from an average VPD daytime proportion. We therefore suggest that extreme climate events of extended time periods of ambient daytime VPD $>$ 1.2 kPa like during the growing season 2018 (Fig. 3b) could reduce the pine forest needle Hg uptake flux in Fennoscandia in future even compared to average long-term VPD projections (Fig. 4).

A source of model uncertainty of the future forest foliar Hg uptake flux under climate change arises from atmospheric Hg(0) concentrations that depend on anthropogenic emissions, re-emissions of mobilized legacy Hg and future global deposition fluxes under climate and land use change (Sonke et al., 2023; Feinberg et al., 2023), which we could not account for in this study. However, our model outputs call attention to the sensi-

tivity of the pine needle Hg uptake flux to extreme hot and dry ambient conditions, which should be accounted for in chemistry-transport models under varying atmospheric Hg(0) levels. The impact of the hot and dry conditions on the pine Hg uptake fluxes might have implications for Hg inputs into aquatic ecosystems. In a recent review on Hg cycling in the context of global change, (Sonke et al., 2023) highlighted the potential of legacy Hg (i.e. actively cycling Hg that was mobilized in the past) to cause contamination by mobilization of Hg from soils to wetlands and coastal ecosystems via riverine systems. While most soil Hg enters riverine systems by soil erosion from agricultural lands, contaminated sites, and deforested woodland (Panagos et al., 2021; Sonke et al., 2023), a reduced forest foliar Hg uptake and subsequent deposition to forest soils may decrease the amount of runoff Hg from forest soils in the long-term, while long-range Hg transport to the open ocean via the atmosphere might be enhanced (Zhou et al., 2021).

3.4 Comparison of bottom-up model with GEOS-Chem

Figure 5 depicts spatial ratios of daily forest Hg uptake fluxes of the bottom-up model to GEOS-Chem. Absolute difference values of the two model outputs are shown in SI Fig. 2.

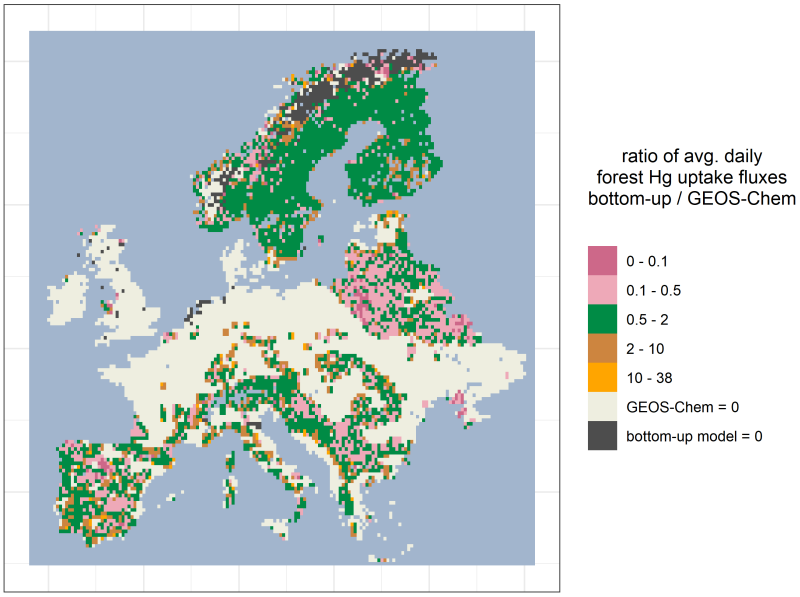

Figure 5. Ratios per spatial unit of daily forest Hg uptake fluxes averaged over the latitude-specific growing season length of the bottom-up model to GEOS-Chem.

Results of average daily foliar Hg uptake fluxes from GEOS-Chem and the bottom-up model were geographically comparable: In 59% of the spatial domain with values > 0, average daily foliar Hg uptake fluxes from the two models differed by factor of 1 - 2 from each other, in 37% of the domain, model values differed by a factor of 2 - 10 from each other, and in 4% of the domain respective values differed by a factor of > 10 from each other (Fig 5). We examined if differences in modelled average daily foliar Hg uptake fluxes at the same geographic location originate from differences in the underlying forest distribution maps of the two compared models. In 78% of spatial tiles with values > 0, the ratio of average daily foliar Hg uptake fluxes of the bottom-up model to GEOS-Chem agreed in range (Fig. 5) with the ratio of the forest fraction of the bottom-up model

to GEOS-Chem per respective spatial tile. We thus hypothesize that the bottom-up model and GEOS-Chem generally produce similar foliar Hg flux values per spatial unit given the same forest distribution. Reasons for minor differences in model outputs are challenging to identify, since the two models are based on different approaches, parameters and underlying maps (Sect. 2.4). For future assessment of model accuracy, we therefore suggest to compare model results to actual measurements of the forest foliar Hg uptake flux (Obrist et al., 2021; Feinberg et al., 2022). The total foliar Hg uptake flux to the European forested area (Fig. 1 and 5) was 22 Mg Hg season^{-1} for GEOS-Chem which almost equals the total flux of 23 $\pm$ 12 Mg Hg season^{-1} for the bottom-up model (Sect. 3.1).

4 Conclusion

We created a highly resolved (1 km^2) map (Fig. 1), which visualizes the spatial variation of foliar Hg uptake fluxes to European forests. The highest foliar Hg uptake fluxes receive Fennoscandia, densely forested areas in Central and Southern Europe , e.g. the Carpathian Mountains, the Balkans, or multiple low mountain areas. We suggest, that this map (Fig. 1) can guide decisions on European background Hg monitoring of the terrestrial environment. The total forest foliar Hg uptake flux over the course of one growing season agrees well with Hg flux estimates derived from literature and from the chemical transport model GEOS-Chem for the same land area of Europe (Fig. 5). This precision among modelling results on a European scale using different approaches gives us confidence that the bottom-up model is overall able to represent the seasonal forest foliar Hg uptake flux. We suggest that the accuracy of modelling results have to be further determined using direct forest foliar Hg flux measurements.

Using an empirical relationship between Hg needle uptake rates of pine trees and VPD threshold exceedance, we found a reduction in modelled pine forest needle Hg uptake flux during the relatively hot and dry growing season in Fennoscandia in 2018 compared to the growing seasons in 1994, 2003 and 2015/2017 (Fig. 2). The modelled average amount of Hg, that was not deposited via pine needle uptake in 2018 compared to the reference time period of 2015/17 exceeded the reported anthropogenic Hg emissions of Sweden in 2021, highlighting the quantitative significance of stomatal Hg uptake. If these hot summer droughts occurred more frequently in Fennoscandia under climate change, the pine forest needle Hg uptake flux would be diminished while these extreme conditions prevail, potentially increasing the Hg burden of the ocean via long-range atmospheric transport. In order to better represent the impact of extreme climate events on the pine forest needle Hg uptake flux, we therefore advise to incorporate a stomatal component of the pine needle Hg uptake flux into chemical transport models like GEOS-Chem.

5 Open Research

Calculated forest foliar Hg uptake fluxes to Europe (Fig. 1) and GEOS-Chem simulation data aggregated to seasonal values are publicly available for download from Zenodo at `https://zenodo.org/record/7851718#.ZFUeLM5Bw2w` and `https://zenodo.org/record/7900753#.ZFUgqM5Bw2w` respectively. All input datasets to the bottom-up model are described in detail in Section 2.1, along with their respective publications and databases, from which the datasets can be accessed. The offline dry deposition code from GEOS-Chem is accessible for download (Feinberg, 2022) and model output data from GEOS-Chem can be obtained from the corresponding author upon request. All calculations and visualizations were done in R, Version 4.0.3.

Acknowledgments

L. Wohlgemuth and M. Jiskra acknowledge financial support from the Swiss National Science Foundation (grant no. 174101). A. Feinberg acknowledges financial support from the Swiss National Science Foundation (Early Postdoc.Mobility grant: P2EZP2 195424) and the US National Science Foundation (#1924148). The GEOS-FP data used in this study/project have been provided by the Global Modeling and Assimilation Office (GMAO) at NASA Goddard Space Flight Center. The evaluation was partly based on data that was collected by partners of the official UNECE ICP Forests Network (http://icp-forests.net/contributors). Part of the ICP Forests data was co-financed by the European Commission. ERA5 and CORDEX data were obtained from the Copernicus Climate Change Service (C3S) Climate Data Store (https://cds.climate.copernicus.eu/cdsapp#!/home). PROBA-V leaf area index values were downloaded from the VITO Product Distribution Portal. Climate calculations under two climate change scenarios (Fig. 2, Fig. 3) were performed at sciCORE (http://scicore.unibas.ch/) scientific computing center at University of Basel.

References

Allen, C. D., Breshears, D. D., & McDowell, N. G. (2015). On underestimation of global vulnerability to tree mortality and forest die-off from hotter drought in the Anthropocene. *Ecosphere*, *6*(8), art129. Retrieved 2021-10-22, from `https://onlinelibrary.wiley.com/doi/abs/10.1890/ES15-00203.1` doi: 10.1890/ES15-00203.1

Berg, A., & Sheffield, J. (2018, June). Climate Change and Drought: the Soil Moisture Perspective. *Curr Clim Change Rep*, *4*(2), 180–191. Retrieved 2021-10-22, from `https://doi.org/10.1007/s40641-018-0095-0` doi: 10.1007/s40641-018-0095-0

Blackwell, B. D., Driscoll, C. T., Maxwell, J. A., & Holsen, T. M. (2014, June). Changing climate alters inputs and pathways of mercury deposition to forested ecosystems. *Biogeochemistry*, *119*(1-3), 215–228. Retrieved 2020-03-10, from `http://link.springer.com/10.1007/s10533-014-9961-6` doi: 10.1007/s10533-014-9961-6

Brando, P. M., Paolucci, L., Ummenhofer, C. C., Ordway, E. M., Hartmann, H., Cattau, M. E., ... Balch, J. (2019, May). Droughts, Wildfires, and Forest Carbon Cycling: A Pantropical Synthesis. *Annu. Rev. Earth Planet. Sci.*, *47*(1), 555–581. Retrieved 2021-10-22, from `https://www.annualreviews.org/doi/10.1146/annurev-earth-082517-010235` doi: 10.1146/annurev-earth-082517-010235

Brus, D. J., Hengeveld, G. M., Walvoort, D. J. J., Goedhart, P. W., Heidema, A. H., Nabuurs, G. J., & Gunia, K. (2012, January). Statistical mapping of tree species over Europe. *European Journal of Forest Research*, *131*(1), 145–157. Retrieved 2019-08-26, from `http://link.springer.com/10.1007/s10342-011-0513-5` doi: 10.1007/s10342-011-0513-5

Buras, A., & Menzel, A. (2019). Projecting Tree Species Composition Changes of European Forests for 2061–2090 Under RCP 4.5 and RCP 8.5 Scenarios. *Frontiers in Plant Science*, *9*, 1986. Retrieved 2021-09-22, from `https://www.frontiersin.org/article/10.3389/fpls.2018.01986` doi: 10.3389/fpls.2018.01986

Buras, A., Rammig, A., & Zang, C. S. (2020, March). Quantifying impacts of the 2018 drought on European ecosystems in comparison to 2003. *Biogeosciences*, *17*(6), 1655–1672. Retrieved 2021-12-07, from `https://bg.copernicus.org/articles/17/1655/2020/` doi: 10.5194/bg-17-1655-2020

C3S. (2022). Copernicus Climate Change Service, Climate Data Store (CDS): CORDEX regional climate model data on single levels. Retrieved from `https://cds.climate.copernicus.eu/cdsapp#!/dataset/10.24381/cds.bc91edc3?tab=overview` doi: 10.24381/cds.bc91edc3

CLRTAP. (2017). Revised Chapter 3 of the Manual on Methodologies and Criteria for Modelling and Mapping Critical Loads and Levels and Air Pollution Effects, Risks and Trends: Mapping Critical Levels for Vegetation. *Umweltbundesamt*. Retrieved from https://www.umweltbundesamt.de/en/manual-for-modelling-mapping-critical-loads-levels doi: https://www.umweltbundesamt.de/en/manual-for-modelling-mapping-critical-loads-levels

Demers, J. D., Blum, J. D., & Zak, D. R. (2013, March). Mercury isotopes in a forested ecosystem: Implications for air-surface exchange dynamics and the global mercury cycle. *Global Biochem. Cy.*, *27*(1), 222–238. Retrieved 2018-11-14, from https://agupubs.onlinelibrary.wiley.com/doi/abs/10.1002/gbc.20021 doi: 10.1002/gbc.20021

Dierckx, W., Sterckx, S., Benhadj, I., Livens, S., Duhoux, G., Van Achteren, T., ... Saint, G. (2014, April). PROBA-V mission for global vegetation monitoring: standard products and image quality. *Int. J. Remote Sens.*, *35*(7), 2589–2614. Retrieved 2021-08-30, from https://doi.org/10.1080/01431161.2014.883097 doi: 10.1080/01431161.2014.883097

Enrico, M., Roux, G. L., Marusczak, N., Heimbürger, L.-E., Claustres, A., Fu, X., ... Sonke, J. E. (2016, March). Atmospheric mercury transfer to peat bogs dominated by gaseous elemental mercury dry deposition. *Environ. Sci. Technol.*, *50*(5), 2405–2412. Retrieved 2019-06-20, from http://pubs.acs.org/doi/10.1021/acs.est.5b06058 doi: 10.1021/acs.est.5b06058

Feinberg, A. (2022). Code reference: arifein/offline-drydep: Offline dry deposition model from GEOS-Chem v1.0 (v1.0). doi: https://doi.org/10.5281/zenodo.6498126

Feinberg, A., Dlamini, T., Jiskra, M., Shah, V., & E. Selin, N. (2022). Evaluating atmospheric mercury (Hg) uptake by vegetation in a chemistry-transport model. *Environmental Science: Processes & Impacts*. Retrieved 2022-07-25, from https://pubs.rsc.org/en/content/articlelanding/2022/em/d2em00032f (Publisher: Royal Society of Chemistry) doi: 10.1039/D2EM00032F

Feinberg, A., Jiskra, M., Borrelli, P., Biswakarma, J., & Selin, N. E. (2023, January). Land use change as an anthropogenic driver of mercury pollution. Retrieved 2023-04-15, from https://eartharxiv.org/repository/view/4963/ (Publisher: EarthArXiv)

Forrester, D. I., Tachauer, I. H. H., Annighoefer, P., Barbeito, I., Pretzsch, H., Ruiz-Peinado, R., ... Sileshi, G. W. (2017, July). Generalized biomass and leaf area allometric equations for European tree species incorporating stand structure, tree age and climate. *Forest Ecology and Management*, *396*, 160–175. Retrieved 2020-06-10, from http://www.sciencedirect.com/science/article/pii/S0378112717301238 doi: 10.1016/j.foreco.2017.04.011

Forzieri, G., Feyen, L., Rojas, R., Flörke, M., Wimmer, F., & Bianchi, A. (2014, January). Ensemble projections of future streamflow droughts in Europe. *Hydrology and Earth System Sciences*, *18*(1), 85–108. Retrieved 2021-12-17, from https://hess.copernicus.org/articles/18/85/2014/ (Publisher: Copernicus GmbH) doi: 10.5194/hess-18-85-2014

Fuster, B., Sánchez-Zapero, J., Camacho, F., García-Santos, V., Verger, A., Lacaze, R., ... Smets, B. (2020, January). Quality assessment of PROBA-V LAI, fAPAR and fCOVER collection 300 m products of Copernicus Global Land Service. *Remote Sens.*, *12*(6), 1017. Retrieved 2021-03-17, from https://www.mdpi.com/2072-4292/12/6/1017 doi: 10.3390/rs12061017

Garonna, I., Jong, R. d., Wit, A. J. W. d., Mücher, C. A., Schmid, B., & Schaepman, M. E. (2014). Strong contribution of autumn phenology to changes in satellite-derived growing season length estimates across Europe (1982–2011). *Glob. Change Biol.*, *20*(11), 3457–3470. Retrieved 2019-10-17, from https://onlinelibrary.wiley.com/doi/abs/10.1111/gcb.12625 doi:

10.1111/gcb.12625

Gharun, M., Hörtnagl, L., Paul-Limoges, E., Ghiasi, S., Feigenwinter, I., Burri, S., ... Buchmann, N. (2020, September). Physiological response of Swiss ecosystems to 2018 drought across plant types and elevation. *Philosophical Transactions of the Royal Society B: Biological Sciences*, *375*(1810), 20190521. Retrieved 2023-04-16, from `https://royalsocietypublishing.org/doi/full/10.1098/rstb.2019.0521` (Publisher: Royal Society) doi: 10.1098/rstb.2019.0521

Gibbs, H. K. (2006). Olson's Major World Ecosystem Complexes Ranked by Carbon in Live Vegetation: an Updated Database Using the GLC2000 Land Cover Product (NDP-017b).
doi: https://www.osti.gov/biblio/1389498

Grossiord, C., Buckley, T. N., Cernusak, L. A., Novick, K. A., Poulter, B., Siegwolf, R. T. W., ... McDowell, N. G. (2020). Plant responses to rising vapor pressure deficit. *New Phytol.*, *226*(6), 1550–1566. Retrieved 2020-09-07, from `https://nph.onlinelibrary.wiley.com/doi/abs/10.1111/nph.16485` doi: 10.1111/nph.16485

Hararuk, O., Obrist, D., & Luo, Y. (2013, April). Modelling the sensitivity of soil mercury storage to climate-induced changes in soil carbon pools. *Biogeosciences*, *10*(4), 2393–2407. Retrieved 2021-10-27, from `https://bg.copernicus.org/articles/10/2393/2013/` doi: 10.5194/bg-10-2393-2013

Hersbach, H., Bell, B., Berrisford, P., Biavati, G., Horányi, A., Muñoz Sabater, J., ... Thépaut, J.-N. (2018). ERA5 hourly data on pressure levels from 1979 to present. Copernicus Climate Change Service (C3S) Climate Data Store (CDS).
doi: 10.24381/cds.bd0915c6

IPCC. (2021a). Climate change 2021. The physical science basis. Working group I contribution to the Sixth Assessment Report of the Intergovernmental Panel on Climate Change.

IPCC. (2021b). Summary for Policymakers. Climate Change 2021: The Physical Science Basis. Contribution of Working Group I to the Sixth Assessment Report of the Intergovernmental Panel on Climate Change. , *Cambride University Press*.

Jacob, D., Teichmann, C., Sobolowski, S., Katragkou, E., Anders, I., Belda, M., ... Wulfmeyer, V. (2020, April). Regional climate downscaling over Europe: perspectives from the EURO-CORDEX community. *Reg Environ Change*, *20*(2), 51. Retrieved 2021-11-03, from `https://doi.org/10.1007/s10113-020-01606-9` doi: 10.1007/s10113-020-01606-9

Jeong, S.-J., Ho, C.-H., Gim, H.-J., & Brown, M. E. (2011). Phenology shifts at start vs. end of growing season in temperate vegetation over the Northern Hemisphere for the period 1982–2008. *Global Change Biology*, *17*(7), 2385–2399. Retrieved 2021-12-20, from `https://onlinelibrary.wiley.com/doi/abs/10.1111/j.1365-2486.2011.02397.x` doi: 10.1111/j.1365-2486.2011.02397.x

Jiskra, M., Sonke, J. E., Obrist, D., Bieser, J., Ebinghaus, R., Myhre, C. L., ... Dommergue, A. (2018). A vegetation control on seasonal variations in global atmospheric mercury concentrations. *Nat. Geosci.*, 1–7. Retrieved from `http:https://doi.org/10.1038/s41561-018-0078-8` doi: 10.1038/s41561-018-0078-8

Jiskra, M., Wiederhold, J. G., Skyllberg, U., Kronberg, R.-M., Hajdas, I., & Kretzschmar, R. (2015). Mercury deposition and re-emission pathways in boreal forest soils investigated with Hg isotope signatures. *Environ. Sci. Technol.*, *49*(12), 7188–7196.

Kellomäki, S., Strandman, H., Heinonen, T., Asikainen, A., Venäläinen, A., & Peltola, H. (2018, March). Temporal and Spatial Change in Diameter Growth

of Boreal Scots Pine, Norway Spruce, and Birch under Recent-Generation (CMIP5) Global Climate Model Projections for the 21st Century. *Forests*, *9*(3), 118. Retrieved 2021-12-16, from https://www.mdpi.com/1999-4907/9/3/118 doi: 10.3390/f9030118

Khan, T., Obrist, D., Agnan, Y., E. Selin, N., & A. Perlinger, J. (2019). Atmosphere-terrestrial exchange of gaseous elemental mercury: parameterization improvement through direct comparison with measured ecosystem fluxes. *Environmental Science: Processes & Impacts*, *21*(10), 1699–1712. Retrieved 2021-10-20, from https://pubs.rsc.org/en/content/articlelanding/2019/em/c9em00341j doi: 10.1039/C9EM00341J

Ku, H. (1966). Notes on the use of propagation of error formulas. *Journal of Research of the National Bureau of Standards*, *70C*(4).

Körner, C. (2013). Plant–Environment Interactions. In A. Bresinsky, C. Körner, J. W. Kadereit, G. Neuhaus, & U. Sonnewald (Eds.), *Strasburger's Plant Sciences: Including Prokaryotes and Fungi* (pp. 1065–1166). Berlin, Heidelberg: Springer. Retrieved 2019-11-25, from https://doi.org/10.1007/978-3-642-15518-5_12

Laacouri, A., Nater, E. A., & Kolka, R. K. (2013, September). Distribution and uptake dynamics of mercury in leaves of common deciduous tree species in Minnesota, U.S.A. *Environ. Sci. Technol.*, *47*(18), 10462–10470. Retrieved 2019-06-20, from http://pubs.acs.org/doi/abs/10.1021/es401357z doi: 10.1021/es401357z

Lagergren, F., & Lindroth, A. (2002, August). Transpiration response to soil moisture in pine and spruce trees in Sweden. *Agr. Forest Meteorol.*, *112*(2), 67–85. Retrieved 2021-08-31, from https://www.sciencedirect.com/science/article/pii/S0168192302000606 doi: 10.1016/S0168-1923(02)00060-6

Liu, Y., Liu, G., Wang, Z., Guo, Y., Yin, Y., Zhang, X., ... Jiang, G. (2021, October). Understanding foliar accumulation of atmospheric Hg in terrestrial vegetation: Progress and challenges. *Critical Reviews in Environmental Science and Technology*, *0*(0), 1–22. Retrieved 2021-10-18, from https://doi.org/10.1080/10643389.2021.1989235 doi: 10.1080/10643389.2021.1989235

Lucchesi, R. (2018). File Specification for GEOS FP. GMAO Office Note No. 4 (Version 1.2). Retrieved from http://gmao.gsfc.nasa.gov/pubs/office_notes

Mauri, A., Strona, G., & San-Miguel-Ayanz, J. (2017, January). EU-Forest, a high-resolution tree occurrence dataset for Europe. *Sci Data*, *4*. Retrieved 2020-01-29, from https://www.ncbi.nlm.nih.gov/pmc/articles/PMC5215058/ doi: 10.1038/sdata.2016.123

Norby, R. J., & Zak, D. R. (2011). Ecological Lessons from Free-Air CO2 Enrichment (FACE) Experiments. *Annual Review of Ecology, Evolution, and Systematics*, *42*(1), 181–203. Retrieved 2021-10-22, from https://doi.org/10.1146/annurev-ecolsys-102209-144647 doi: 10.1146/annurev-ecolsys-102209-144647

Obrist, D., Agnan, Y., Jiskra, M., Olson, C. L., Colegrove, D. P., Hueber, J., ... Helmig, D. (2017, July). Tundra uptake of atmospheric elemental mercury drives Arctic mercury pollution. *Nature*, *547*(7662), 201–204. Retrieved 2019-06-24, from http://www.nature.com/articles/nature22997 doi: 10.1038/nature22997

Obrist, D., Roy, E. M., Harrison, J. L., Kwong, C. F., Munger, J. W., Moosmüller, H., ... Commane, R. (2021, July). Previously unaccounted atmospheric mercury deposition in a midlatitude deciduous forest. *PNAS*, *118*(29). Retrieved 2021-07-26, from https://www.pnas.org/content/118/29/e2105477118 doi: 10.1073/pnas.2105477118

Oksanen, E., Lihavainen, J., Keinänen, M., Keski-Saari, S., Kontunen-Soppela, S., Sellin, A., & Sõber, A. (2019). Northern Forest Trees Under Increasing Atmospheric Humidity. In F. M. Cánovas, U. Lüttge, R. Matyssek, & H. Pretzsch

(Eds.), *Progress in Botany Vol. 80* (pp. 317–336). Cham: Springer International Publishing. Retrieved 2021-12-17, from https://doi.org/10.1007/124_2017_15

Pan, Y., Birdsey, R. A., Phillips, O. L., & Jackson, R. B. (2013, November). The Structure, Distribution, and Biomass of the World's Forests. *Annu. Rev. Ecol. Evol. Syst.*, *44*(1), 593–622. Retrieved 2022-01-10, from https://www.annualreviews.org/doi/10.1146/annurev-ecolsys-110512-135914 doi: 10.1146/annurev-ecolsys-110512-135914

Panagos, P., Jiskra, M., Borrelli, P., Liakos, L., & Ballabio, C. (2021, October). Mercury in European topsoils: Anthropogenic sources, stocks and fluxes. *Environmental Research*, *201*, 111556. Retrieved 2021-07-29, from https://www.sciencedirect.com/science/article/pii/S0013935121008501 doi: 10.1016/j.envres.2021.111556

Panek, J. A., & Goldstein, A. H. (2001, March). Response of stomatal conductance to drought in ponderosa pine: implications for carbon and ozone uptake. *Tree Physiol.*, *21*(5), 337–344. Retrieved 2021-07-22, from https://doi.org/10.1093/treephys/21.5.337 doi: 10.1093/treephys/21.5.337

Papula, L. (2003). *Mathematische Formelsammlung für Ingenieure und Naturwissenschaftler* (8th ed.). Vieweg.

Pleijel, H., Klingberg, J., Nerentorp, M., Broberg, M. C., Nyirambangutse, B., Munthe, J., & Wallin, G. (2021, December). Mercury accumulation in leaves of different plant types – the significance of tissue age and specific leaf area. *Biogeosciences*, *18*(23), 6313–6328. Retrieved 2021-12-23, from https://bg.copernicus.org/articles/18/6313/2021/ doi: 10.5194/bg-18-6313-2021

Rea, A. W., Lindberg, S. E., Scherbatskoy, T., & Keeler, G. J. (2002). Mercury accumulation in foliage over time in two northern mixed-hardwood forests. *Water Air Soil Poll.*, *133*, 49–67.

Rutter, A. P., Schauer, J. J., Shafer, M. M., Creswell, J. E., Olson, M. R., Robinson, M., ... Mallek, J. L. (2011, February). Dry deposition of gaseous elemental mercury to plants and soils using mercury stable isotopes in a controlled environment. *Atmos. Environ.*, *45*(4), 848–855. Retrieved 2019-09-24, from http://www.sciencedirect.com/science/article/pii/S1352231010009805 doi: 10.1016/j.atmosenv.2010.11.025

Samaniego, L., Thober, S., Kumar, R., Wanders, N., Rakovec, O., Pan, M., ... Marx, A. (2018, May). Anthropogenic warming exacerbates European soil moisture droughts. *Nature Clim Change*, *8*(5), 421–426. Retrieved 2021-12-17, from https://www.nature.com/articles/s41558-018-0138-5 doi: 10.1038/s41558-018-0138-5

Selin, N. E., Jacob, D. J., Yantosca, R. M., Strode, S., Jaeglé, L., & Sunderland, E. M. (2008). Global 3-D land-ocean-atmosphere model for mercury: Present-day versus preindustrial cycles and anthropogenic enrichment factors for deposition. *Global Biogeochemical Cycles*, *22*(2). Retrieved 2020-09-22, from https://agupubs.onlinelibrary.wiley.com/doi/abs/10.1029/2007GB003040 doi: 10.1029/2007GB003040

Smith-Downey, N. V., Sunderland, E. M., & Jacob, D. J. (2010). Anthropogenic impacts on global storage and emissions of mercury from terrestrial soils: Insights from a new global model. *Journal of Geophysical Research: Biogeosciences*, *115*(G3). Retrieved 2019-06-20, from https://agupubs.onlinelibrary.wiley.com/doi/abs/10.1029/2009JG001124 doi: 10.1029/2009JG001124

Sonke, J. E., Angot, H., Zhang, Y., Poulain, A., Björn, E., & Schartup, A. (2023, May). Global change effects on biogeochemical mercury cycling. *Ambio*, *52*(5), 853–876. Retrieved 2023-04-15, from https://doi.org/10.1007/s13280-023-01855-y doi: 10.1007/s13280-023-01855-y

Stocker, B. D., Zscheischler, J., Keenan, T. F., Prentice, I. C., Seneviratne, S. I., & Peñuelas, J. (2019, April). Drought impacts on terrestrial primary production underestimated by satellite monitoring. *Nat. Geosci.*, *12*(4), 264–270. Retrieved 2021-10-22, from https://www.nature.com/articles/s41561-019-0318-6 doi: 10.1038/s41561-019-0318-6

Wang, Q., Tenhunen, J., Dinh, N., Reichstein, M., Otieno, D., Granier, A., & Pilegarrd, K. (2005, June). Evaluation of seasonal variation of MODIS derived leaf area index at two European deciduous broadleaf forest sites. *Remote Sensing of Environment*, *96*(3-4), 475–484. Retrieved 2019-05-15, from https://linkinghub.elsevier.com/retrieve/pii/S0034425705001252 doi: 10.1016/j.rse.2005.04.003

Wang, R., Chen, J. M., Liu, Z., & Arain, A. (2017, August). Evaluation of seasonal variations of remotely sensed leaf area index over five evergreen coniferous forests. *ISPRS Journal of Photogrammetry and Remote Sensing*, *130*, 187–201. Retrieved 2020-10-13, from http://www.sciencedirect.com/science/article/pii/S0924271616305998 doi: 10.1016/j.isprsjprs.2017.05.017

Wang, Y., Jacob, D. J., & Logan, J. A. (1998). Global simulation of tropospheric O3-NO x -hydrocarbon chemistry: 1. Model formulation. *Journal of Geophysical Research: Atmospheres*, *103*(D9), 10713–10725. Retrieved 2022-05-25, from https://onlinelibrary.wiley.com/doi/abs/10.1029/98JD00158 (_eprint: https://onlinelibrary.wiley.com/doi/pdf/10.1029/98JD00158) doi: 10.1029/98JD00158

Wesely, M. L. (2007, January). Parameterization of surface resistances to gaseous dry deposition in regional-scale numerical models. *Atmospheric Environment*, *41*, 52–63. Retrieved 2021-10-21, from https://www.sciencedirect.com/science/article/pii/S1352231007009740 doi: 10.1016/j.atmosenv.2007.10.058

Wohlgemuth, L., Osterwalder, S., Joseph, C., Kahmen, A., Hoch, G., Alewell, C., & Jiskra, M. (2020, December). A bottom-up quantification of foliar mercury uptake fluxes across Europe. *Biogeosciences*, *17*(24), 6441–6456. Retrieved 2021-01-14, from https://bg.copernicus.org/articles/17/6441/2020/ doi: https://doi.org/10.5194/bg-17-6441-2020

Wohlgemuth, L., Rautio, P., Ahrends, B., Russ, A., Vesterdal, L., Waldner, P., ... Jiskra, M. (2022, March). Physiological and climate controls on foliar mercury uptake by European tree species. *Biogeosciences*, *19*(5), 1335–1353. Retrieved 2022-03-14, from https://bg.copernicus.org/articles/19/1335/2022/ (Publisher: Copernicus GmbH) doi: 10.5194/bg-19-1335-2022

Wu, Z., Wang, X., Chen, F., Turnipseed, A. A., Guenther, A. B., Niyogi, D., ... Alapaty, K. (2011, May). Evaluating the calculated dry deposition velocities of reactive nitrogen oxides and ozone from two community models over a temperate deciduous forest. *Atmospheric Environment*, *45*(16), 2663–2674. Retrieved 2021-10-21, from https://www.sciencedirect.com/science/article/pii/S1352231011002275 doi: 10.1016/j.atmosenv.2011.02.063

Yuan, H., Dai, Y., Xiao, Z., Ji, D., & Shangguan, W. (2011, May). Reprocessing the MODIS Leaf Area Index products for land surface and climate modelling. *Remote Sensing of Environment*, *115*(5), 1171–1187. Retrieved 2023-04-16, from https://www.sciencedirect.com/science/article/pii/S0034425711000149 doi: 10.1016/j.rse.2011.01.001

Yuan, W., Sommar, J., Lin, C.-J., Wang, X., Li, K., Liu, Y., ... Feng, X. (2019, January). Stable isotope evidence shows re-emission of elemental mercury vapor occurring after reductive loss from foliage. *Environ. Sci. Technol.*, *53*(2), 651–660. Retrieved 2019-11-29, from https://doi.org/10.1021/acs.est.8b04865 doi: 10.1021/acs.est.8b04865

Yuan, W., Zheng, Y., Piao, S., Ciais, P., Lombardozzi, D., Wang, Y., ... Yang, S. (2019, August). Increased atmospheric vapor pressure deficit re-

duces global vegetation growth. *Sci. Adv.*, *5*(8). Retrieved 2019-09-06, from https://advances.sciencemag.org/content/5/8/eaax1396 doi: 10.1126/sciadv.aax1396

Zhang, H., Holmes, C., & Wu, S. (2016, September). Impacts of changes in climate, land use and land cover on atmospheric mercury. *Atmospheric Environment*, *141*, 230–244. Retrieved 2021-10-21, from https://linkinghub.elsevier.com/retrieve/pii/S1352231016304897 doi: 10.1016/j.atmosenv.2016.06.056

Zhang, L., Wright, L. P., & Blanchard, P. (2009, December). A review of current knowledge concerning dry deposition of atmospheric mercury. *Atmos. Environ.*, *43*(37), 5853–5864. Retrieved 2019-10-03, from http://www.sciencedirect.com/science/article/pii/S1352231009007407 doi: 10.1016/j.atmosenv.2009.08.019

Zhou, J., & Obrist, D. (2021). Global mercury assimilation by vegetation. *Environ. Sci. Technol.*. Retrieved 2021-10-08, from https://doi.org/10.1021/acs.est.1c03530 doi: 10.1021/acs.est.1c03530

Zhou, J., Obrist, D., Dastoor, A., Jiskra, M., & Ryjkov, A. (2021, March). Vegetation uptake of mercury and impacts on global cycling. *Nat. Rev. Earth Environ.*, 1–16. Retrieved 2021-03-16, from https://www.nature.com/articles/s43017-021-00146-y doi: 10.1038/s43017-021-00146-y

Zweifel, R., Rigling, A., & Dobbertin, M. (2009). Species-specific stomatal response of trees to drought – a link to vegetation dynamics? *J. Veg. Sci.*, *20*(3), 442–454. Retrieved 2021-09-08, from https://onlinelibrary.wiley.com/doi/abs/10.1111/j.1654-1103.2009.05701.x doi: 10.1111/j.1654-1103.2009.05701.x

Zweifel, R., Steppe, K., & Sterck, F. J. (2007, June). Stomatal regulation by microclimate and tree water relations: interpreting ecophysiological field data with a hydraulic plant model. *J. Exp. Bot.*, *58*(8), 2113–2131. Retrieved 2021-04-19, from https://doi.org/10.1093/jxb/erm050 doi: 10.1093/jxb/erm050

https://www.overleaf.com/project/623c4a3b9809e1d1d1117124

A spatial assessment of current and future foliar Hg uptake fluxes across European forests

Lena Wohlgemuth[1,2], Aryeh Feinberg[3], Allan Buras[4], Martin Jiskra[1]

[1]Department of Environmental Geosciences, University of Basel, Basel, Switzerland
[2]Thünen Institute of Forest Ecosystems, Eberswalde, Germany
[3]Institute for Data, Systems, and Society, MIT, Cambridge, USA
[4]TUM School of Life Sciences, Technical University of Munich, Munich, Germany

Key Points:

- Extreme hot and dry atmospheric conditions have the potential to reduce stomatal uptake of ambient mercury by pine trees in Europe
- Atmospheric drought controls on stomatal mercury uptake should be accounted for in mercury transport models like GEOS-Chem
- Forest foliar mercury uptake fluxes to Europe from a bottom-up model generally agree well with results derived from literature and GEOS-Chem

Corresponding author: Lena Wohlgemuth, `lena.wohlgemuth@thuenen.de`

Abstract

Atmospheric mercury (Hg) is deposited to land surfaces mainly through vegetation uptake. Foliage stomatal gas exchange plays an important role for net vegetation Hg uptake, because foliage assimilates Hg via the stomata. Here, we use empirical relationships of foliar Hg uptake by forest tree species to produce a spatially highly resolved (1 km^2) map of foliar Hg fluxes to European forests over one growing season. The modelled forest foliar Hg uptake flux is 23 ± 12 Mg Hg $season^{-1}$, which agrees with previous estimates from literature.

We spatially compare forest Hg fluxes with modelled fluxes of the chemistry-transport model GEOS-Chem and find a good overall agreement. For European pine forests, stomatal Hg uptake was shown to be sensitive to prevailing conditions of relatively high ambient water vapor pressure deficit (VPD). We tested a stomatal uptake model for the total pine needle Hg uptake flux during four previous growing seasons (1994, 2003, 2015/2017, 2018) and two climate change scenarios (RCP 4.5 and RCP 8.5). The resulting modelled total European pine needle Hg uptake fluxes are in a range of 8.0 - 9.3 Mg Hg $season^{-1}$ (min - max). The lowest pine forest needle Hg uptake flux to Europe (8 Mg Hg $season^{-1}$) among all investigated growing seasons is associated with unusually hot and dry ambient conditions in the European summer 2018, highlighting the sensitivity of the investigated flux to prolonged high VPD. We conclude, that stomatal modelling is particularly useful to investigate changes in Hg deposition in the context of extreme climate events.

1 Introduction

Mercury (Hg) is a toxic pollutant that is transported globally through the atmosphere and deposited from air to land surfaces mainly through vegetation uptake of ambient gaseous elemental Hg(0) (Demers et al., 2013; Jiskra et al., 2015; Enrico et al., 2016; Obrist et al., 2017; Feinberg et al., 2022). Consequently, vegetation uptake has the potential to lower atmospheric Hg(0) transport and Hg deposition to oceans, where Hg can be methylated and bioaccumulated in marine seafood for human consumption (Zhou et al., 2021). In order to assess and improve the effectiveness of mitigation policies for human exposure, it is thus necessary to constrain environmental drivers of vegetation Hg(0) uptake. Furthermore, process understanding of vegetation Hg(0) uptake is essential for assessing future human Hg exposure in the context of global change (Sonke et al., 2023).

Global vegetation and soil uptake of Hg(0) has been estimated to amount to 2850 ± 500 Mg $year^{-1}$ (Obrist et al., 2021; Zhou et al., 2021; Feinberg et al., 2022), exceeding approximate direct anthropogenic emissions to the air of 2200 Mg Hg $year^{-1}$ (Sonke et al., 2023). Forests contain 80 % of the global plant biomass (Pan et al., 2013), therefore representing a major vector for Hg(0) drawdown from the atmosphere. In forests, half of the total Hg(0) net deposition is estimated to be stored in tree foliage, while the other half is estimated to be transferred to vascular tissues (e.g. stem, branches, roots), or taken up by understory vegetation (e.g. shrubs, grasses) or nonvascular plants (lichen and mosses) (Zhou et al., 2021; Obrist et al., 2021; Zhou & Obrist, 2021). In tree foliage, Hg concentrations increase linearly between foliage emergence and senescence (Rea et al., 2002; Laacouri et al., 2013; Blackwell et al., 2014; Wohlgemuth et al., 2020; Pleijel et al., 2021) implying a net foliar Hg deposition flux, albeit Hg re-emission from foliar surfaces of up to 30% of gross foliage Hg(0) deposition had been observed in a subtropical forest in China (W. Yuan, Sommar, et al., 2019). The bulk (90-96%) of Hg is stored in foliage tissues as opposed to leaf surfaces and correlates with leaf stomatal density (Laacouri et al., 2013). Studies on Hg stable isotopes in foliage (Demers et al., 2013; Zhou et al., 2021), enriched isotope tracer experiments (Rutter et al., 2011) and the vertical variation of net foliar Hg uptake in forest canopies (Wohlgemuth et al., 2020) strongly suggest a diffusive uptake pathway of atmospheric Hg(0) to foliage interiors via the stomata (Liu et al., 2021). In this way, foliar Hg(0) uptake is linked to foliage stomatal aperture for atmospheric gas exchange (Wohlgemuth et al., 2022).

Trees regulate foliage stomatal aperture to balance the inward diffusion of CO_2 for photosynthesis with the risk of desiccation caused by excessive outward diffusion of water vapor (Körner, 2013). The degree of stomatal aperture depends on atmospheric CO_2 levels and hydrological conditions (soil water availability and atmospheric evaporative demand) and varies among foliage-specific traits (age, tree species-specific evolutionary metabolic strategy and water use efficiency) (Körner, 2013). Pine, for instance, is an isohydric tree species capable of closing foliage stomata under warm and dry atmospheric conditions relatively early compared to tree species like oak and spruce (Lagergren & Lindroth, 2002; Zweifel et al., 2007, 2009), resulting in a reduced stomatal conductance for pine needle diffusive gas exchange (Panek & Goldstein, 2001). Consistently, Hg(0) uptake rates by pine needles in Europe were found to be lower at forest sites across Europe, where prolonged warm and dry atmospheric conditions prevailed over a given growing season during daytime (Wohlgemuth et al., 2022).

Species-specific stomatal response strategies to meteorological conditions are particularly relevant for projections of future foliar Hg uptake under climate change. Increasing global atmospheric temperatures driven by rising levels of greenhouse gases will result in an increased frequency of droughts (Grossiord et al., 2020) and higher soil moisture deficits (Berg & Sheffield, 2018; Stocker et al., 2019) in various regions of the world. These climatic conditions may decrease foliar Hg(0) uptake fluxes due to lower stomatal conductance (Wohlgemuth et al., 2022). A reduced plant Hg sink could further be amplified by deforestation and forest diebacks, particularly in the tropics (Allen et al., 2015; Brando et al., 2019; Feinberg et al., 2023). Other regions of the world are projected to become wetter through an increase in precipitation rates under climate change (IPCC, 2021a), which might lead to higher foliage stomatal conductance relative to the present and thus higher foliar Hg uptake. With continuing anthropogenic carbon emissions, an elevated atmospheric CO_2 level might have an antagonizing effect on the foliar stomatal Hg(0) uptake flux: foliar Hg(0) uptake could decline with decreasing stomatal conductance under CO_2 fertilization (Norby & Zak, 2011), or, the opposite, the vegetation sink for Hg(0) could increase with intensified biomass growth and higher soil C contents (Hararuk et al., 2013; Jiskra et al., 2018; H. Zhang et al., 2016). In order to make projections of the foliar Hg uptake flux in the next decades, these climate change impacts need to be further investigated and potentially implemented into global and regional Hg cycle models.

Current and future Hg fluxes are modelled in Global Chemical Transport Models (CTMs). CTMs like GEOS-Chem (Selin et al., 2008) apply resistance-based algorithms (Wesely, 2007) for modelling Hg(0) deposition fluxes from the atmosphere to vegetated ecosystems and are often based on parameters like leaf area indices (LAIs), temperature and wind speed. The resistance components for leaf stomata within CTMs commonly represent consensus values optimized to fit observations of Hg deposition velocities over vegetated surfaces (Selin et al., 2008; L. Zhang et al., 2009; Smith-Downey et al., 2010; H. Zhang et al., 2016), without taking stomatal feedback to environmental conditions into account (Wu et al., 2011; Khan et al., 2019). Consequently, forest tree species-specific stomatal responses to climate change at foliage level are not parameterized in CTMs. An additional problem related to CTMs is the uncertainty of modelled Hg(0) deposition fluxes due to insufficient model evaluation against dry deposition measurements (Feinberg et al., 2022). This issue of model validation was highlighted in a recent revision of GEOS-Chem parameterization after matching the GEOS-Chem model design to various experimental Hg(0) deposition measurements, which resulted in a doubling of the modelled global flux of Hg(0) dry deposition to land compared to previous model outcomes (Feinberg et al., 2022).

In this study, we assess the spatial variation of forest foliar Hg uptake fluxes across Europe by producing a spatially highly resolved map of foliar Hg uptake fluxes to European forests using a bottom-up model that incorporates pine tree stomatal responses to climate conditions. We compare these spatially resolved fluxes to forest dry deposition fluxes modelled in GEOS-Chem in order to identify spatial discrepancies between

GEOS-Chem and the bottom-up model used here. We investigate the sensitivity of an empirical stomatal response model of pine to different climatic conditions during past growing seasons and for two climate change projections of the years 2068 - 2082 in order to outline the potential of incorporating a stomatal response function into CTMs.

2 Materials and Methods

2.1 Description of datasets

For creating maps of foliar and pine needle Hg uptake fluxes in Europe applying a bottom-up model (Sect. 2.2 and 2.3), we drew on multiple data sources:

- **Foliar Hg data**. A dataset of foliar Hg uptake rates was derived from Hg measurements in foliage of tree canopies at 272 forest sites of the UNECE International Co-operative Programme on Assessment and Monitoring of Air Pollution Effects on Forests (ICP Forests). Forest sites are mostly located in Central and Northern Europe (+ 737 sites in Austria from the Austrian Bio-Indicator Grid) and harmonized foliage sampling methods were employed. All foliage samples within this dataset were harvested at the end of the growing seasons 2015 or 2017. Therefore, average foliage values of 2015/2017 constitute reference values of forest foliar Hg uptake fluxes relative to respective fluxes during investigated years of this study. The dataset is publicly available and contains 3569 foliar Hg concentrations of 23 tree species and is described in detail in (Wohlgemuth et al., 2022).
- **Meteorological data**. Values on ambient temperature and relative humidity at surface air pressure (1000 hPa) in Europe (spatial resolution: 0.25° x 0.25°) originate from ERA5 hourly reanalysis data and were downloaded from the Copernicus Climate Data Store (Hersbach et al., 2018). The applied time frame includes hourly daytime (07:00 - 18:00 LT) values during the respective growing seasons (April - October) of 1994, 2003, 2015, 2017, and 2018.
- **Climate change data**. Regional climate simulation data of air temperature and relative humidity at 2 m above surface level for the years 2068 - 2082 and two different climate change scenarios (Representative Concentration Pathway (RCP) 4.5 and RCP 8.5 (IPCC, 2021b)) were obtained from the Coordinated Regional Climate Downscaling Experiment (CORDEX) (Jacob et al., 2020) framework for the European domain with a spatial resolution of 0.11° x 0.11° and a temporal resolution of 3hourly daytime (09:00 - 18:00 LT) values. For representing a range of different climate model outputs, we calculated average values from multiple regional climate models (RCMs) downscaled from global climate models (GCMs) depending on availability for download from the Copernicus Climate Data Store (C3S, 2022). In total, we incorporated data of 15 combinations of 4 RCMs and 6 GCMs for RCP 4.5 and of 13 combinations of 6 RCMs and 8 GCMs for RCP 8.5 (see Table SI 3) for an overview of models and ensemble members).
- **European tree species distribution**. We used a map of spatial proportions of tree species groups per km^2 land area from (Brus et al., 2012). For use in calculating pine foliar Hg uptake fluxes (see Sect. 2.3), we summed up spatial relative abundance values of *Pinus sylvestris*, *Pinus pinaster*, *Pinus nigra* and *Pinus halepensis* from European forest inventories (Mauri et al., 2017; Buras & Menzel, 2019) and multiplied these pine relative abundances with the respective total forest area per km^2 derived from (Brus et al., 2012) to obtain pine areal proportions. We performed the same calculation (sum of values of *Pinus sylvestris*, *Pinus pinaster*, *Pinus nigra* and *Pinus halepensis* and subsequent multiplication with respective total forest area) to estimate the distribution of pine in Europe under climate change using relative abundance probabilities projected from climate analogues for the time period 2061 - 2090 and RCP 4.5 and RCP 8.5 by (Buras & Menzel, 2019).

- **Leaf Area Indices (LAIs) and Leaf Mass per Area (LMA) values**. We used the LAI satellite product (spatial resolution: 330 m) of PROBA-V (Dierckx et al., 2014; Fuster et al., 2020) to upscale foliar Hg uptake rates at each ICP Forests site to foliar Hg uptake fluxes (see Sect. 2.2), along with average LMA values per tree species from (Forrester et al., 2017).

2.2 Calculation of forest foliage Hg uptake fluxes

We determined forest foliar Hg uptake fluxes to European forests on a 1 km^2 spatial resolution applying three basic computational steps: 1) calculation of tree species-specific daily Hg uptake fluxes per m^2 ground area using a bottom-up model; 2) upscaling of respective foliar Hg fluxes per tree species to the European forested area using the areal distribution of corresponding tree species; 3) multiplication of daily forest foliar Hg uptake fluxes per latitude with latitude-dependent growing season length in order to obtain the forest foliar Hg uptake fluxes over one growing season.

Computational step 1) is based on the premise, that foliar Hg uptake rates are tree species-specific (Laacouri et al., 2013; Wohlgemuth et al., 2022; Pleijel et al., 2021). For this reason, we calculated median daily foliar Hg uptake fluxes per tree species group (see Table SI 2 for details) of all forest sites from the foliar Hg dataset (Sect. 2.1). The bottom-up modeling approach for calculating daily foliar Hg uptake fluxes from daily foliar Hg uptake rates is described in detail in Wohlgemuth et al., (2020) (Wohlgemuth et al., 2020). Briefly, daily foliar Hg uptake rates per gram foliage dry weight (units of ng Hg $g_{d.w.}^{-1}$ d^{-1}) were multiplied with tree species-specific LMA values (Sect. 2.1) to obtain daily foliar Hg uptake rates per foliage surface area (ng Hg m_{leaf}^{-2} d^{-1}). Subsequently, values of daily foliar Hg uptake rates per foliage surface area are multiplied with values of LAI (m_{leaf}^{2} m_{ground}^{-2}; Sect. 2.1), resulting in daily foliar Hg fluxes per unit ground area (ng Hg m_{ground}^{-2} d^{-1}). LAI values of coniferous forests are relatively constant during the active growing season after the initial growth phase of current-season needles (R. Wang et al., 2017), while LAI values of temperate deciduous forests increase rapidly at the beginning of the growing season (leaf flushing) and climax at peak season (June – August, northern hemisphere) (Q. Wang et al., 2005). For coniferous tree species, we used the maximum LAI value during the constant period at each forest site of the ICP Forests dataset to calculate needle foliar Hg uptake fluxes. For deciduous tree species, we calculated foliar Hg uptake fluxes as a temporal sequence at every LAI value available over the growing season and subsequently used median foliar Hg uptake flux values of the growing season. For LAI values larger than 3, we applied a species-specific tree height correction factor, to account for lower foliar Hg uptake fluxes of shaded leaves in the lower canopy (Wohlgemuth et al., 2020) (refer to Table SI 1 for utilized tree height correction factors). For coniferous species, we multiplied Hg uptake fluxes of current-season needles with a species-specific needle age correction factor to account for lower Hg uptake rates of older needle age classes (Wohlgemuth et al., 2020) (refer to Table SI 1 for utilized needle age correction factors).

Computational step 2) involves the multiplication of the proportion of each tree species per km^2 land area with the respective species-specific median daily foliar Hg uptake fluxes. We matched tree species-specific Hg data with the areal forest distribution of the respective tree species (Brus et al., 2012). In the few cases of rare European tree species, where specific Hg data was lacking, we pooled Hg or forest distribution data by tree species group (see Table SI 2 for an overview of matched tree species groups between the two datasets). Subsequently, we added up all tree species-specific daily foliar Hg uptake fluxes within each km^2 and obtained one forest foliar daily Hg uptake flux per km^2.

In computational step 3) we calculated forest foliar Hg uptake fluxes per km^2 and one growing season by multiplying each daily foliar Hg uptake flux per km^2 with the growing season length in days following a simple latitudinal model (CLRTAP, 2017). The latitudinal model of growing season determines a growing season length of 192 days at latitude 50° and decreases by 3.5 days per 1° of latitude moving north and increases by 3.5 days per 1° of latitude moving south.

2.3 Calculation of pine foliar Hg uptake fluxes

Daily foliar Hg uptake rates of pine tree species were calculated taking into account the empirical dependence of needle Hg uptake fluxes to atmospheric VPD. Pine needle daily Hg uptake rates (upR_{pine}; ng Hg $g_{d.w.}^{-1}$ d^{-1}) were found to be lower at forest sites, where the daytime fraction of water VPD > 1.2 kPa during the respective sample life period ($proportion_{dayVPD} > 1.2$kPa) was relatively high (Wohlgemuth et al., 2022). The negative correlation of pine needle Hg uptake with timespan of elevated atmospheric VPD was explained by a stomatal closure upon VPD threshold exceedance and thus a high stomatal resistance suppressing the diffusive uptake of Hg(0) from the atmosphere. The linear regression of daily foliar Hg uptake rates with $proportion_{dayVPD} > 1.2$ kPa is: upR_{pine} = 0.116 – 0.13 x ($proportion_{dayVPD} > 1.2$ kPa) (Wohlgemuth et al., 2022). We applied this linear relationship to calculate the pine foliar Hg uptake rates of the forest area of Europe during four different growing seasons in 1994, 2003, an average of 2015 and 2017, 2018, and projected for the time period 2068 - 2082 under RCP 4.5 and RCP 8.5 (IPCC, 2021b). We calculated hourly or 3hourly daytime VPD values from ERA5 (Hersbach et al., 2018) or CORDEX data (Sect. 2.1) on surface temperature and relative humidity using the Auguste-Roche-Magnus formula (W. Yuan, Zheng, et al., 2019) and subsequently determining the fraction of daytime hours when the VPD was above the threshold of 1.2 kPa over the respective latitudinal growing season length. Calculations with climate data were performed at sciCORE scientific computing center at University of Basel. We defined growing season length per latitude using a latitudinal model ((CLRTAP, 2017), see Sect. 2.2). In 2068 - 2082 we assumed the beginning of the growing season to be 3 days earlier and the end of the growing season to be 3 days later to take increases in growing season length under climate change into account (Jeong et al., 2011; Garonna et al., 2014). The underlying areal distribution of pine is based on European forest inventories and projections of pine abundances based on climate analogues under RCP 4.5 and RCP 8.5 by (Buras & Menzel, 2019) (see Sect. 2.1).

2.4 GEOS-Chem forest deposition flux calculation

GEOS-Chem is a global 3-D chemistry transport model, which includes a comprehensive Hg cycle (Selin et al., 2008). Table 1 gives an overview of the methodological approach and input parameters for calculating the respective Hg fluxes of GEOS-Chem and the bottom-up model (Sect. 2.2), which we compared spatially in this study.

Table 1. Caption

	bottom-up model	**GEOS-Chem**
model input parameters	spatial forest distribution (Brus et al., 2012); leaf area indices (LAIs) (Dierckx et al., 2014; Fuster et al., 2020); leaf mass per area (LMA) (Forrester et al., 2017); meteorological parameter: daytime VPD (Hersbach et al., 2018); foliar Hg uptake rates (Wohlgemuth et al., 2022)	spatial forest distribution (Gibbs, 2006); leaf area indices (LAIs) (H. Yuan et al., 2011); atmospheric Hg(0) levels (GEOS-Chem v12.8.1 simulation 2015); meteorological parameters: air temperature, pressure, solar radiation, cloud cover, wind speed (GEOS-FP) (Lucchesi, 2018)
spatial resolution	1 km x 1 km	0.25 x 0.3125°
basic methodological approach for Hg flux calculation	spatial upscaling of measured foliar Hg uptake rates (Wohlgemuth et al., 2020)	in-series calculation of Hg dry deposition velocity from parameterized resistance values (Wesely, 2007)
foliage stomatal Hg uptake flux component	calculated for pine based on daytime vapor pressure deficit (VPD) values (Sect. 2.3)	calculated within the canopy resistance component as a function of land type, leaf area indices (LAIs), and solar radiation
model output compared in this study	tree-species specific forest foliar Hg(0) uptake fluxes	Hg(0) dry deposition fluxes to coniferous and deciduous forest land cover

We used an offline version of the GEOS-Chem dry deposition code (Feinberg, 2022) to be able to calculate dry deposition velocities at higher resolution and only for certain land use types (i.e., forest areas). The offline dry deposition code computes deposition velocities using a resistance-based approach (Y. Wang et al., 1998; Wesely, 2007). Input variables (Table 1) are gridded hourly GEOS-FP meteorological data for (e.g., air temperature, wind speed, solar radiation, and cloud cover) and weekly LAI values based on MODIS (H. Yuan et al., 2011) for the year 2015. The model calculates the Hg(0) dry deposition velocity based on species-specific parameters including its biological reactivity ($f_0 = 10^{-5}$) and Henry's Law Constant ($H^* = 0.11$ M atm^{-1}). To isolate the uptake of Hg(0) to forests, we calculated the dry deposition velocity only over coniferous and deciduous land cover types from the Olson land map (Gibbs, 2006). The offline calculations output hourly dry deposition velocities over the European domain at $0.25 \times 0.3125°$ resolution. We converted the calculated Hg(0) deposition velocities to fluxes by multiplying with hourly surface Hg(0) concentrations from a GEOS-Chem v12.8.1 simulation for 2015. For this study, we compared the GEOS-Chem Hg(0) dry deposition fluxes to forests with foliar Hg(0) uptake fluxes calculated using the bottom-up model. For both models, Hg fluxes were averaged over the latitude-dependent growing season length in days and cropped to the same spatial extent. As GEOS-Chem and the bottom-up model differ in their geographic resolution (GEOS-Chem: 0.25° x 0.31° $\sim$ 955 km^2 vs. bottom-up: 1 km^2), we downsampled daily forest foliar Hg uptake fluxes from the bottom-up model through bilinear interpolation.

2.5 Uncertainty analysis of foliar Hg uptake fluxes

The relative uncertainty value per tree species group depended on propagated uncertainties of calculation parameters used to derive the respective foliar Hg uptake flux per tree species group (see Table SI 4 for details and values). Subsequently, we calculated one relative uncertainty value per geographic tile of our European flux map (Fig. 1) by summarizing the relative uncertainty of each foliar Hg uptake flux per tree species group within each tile according to error propagation principles (Ku, 1966; Papula, 2003). We obtained the relative uncertainty for the total foliar Hg uptake flux to European forests (Fig. 1) by propagating all relative uncertainty values per tile. The final relative uncertainty value of total foliar Hg uptake flux to European forests and the reference growing seasons 2015/2017 is 0.52.

3 Results and Discussion

3.1 Spatial distribution of forest foliar Hg uptake fluxes across Europe

Figure 1 visualizes forest foliar Hg uptake fluxes per growing season at a spatial resolution of 1 km^2 (g Hg km^{-2} season^{-1}) in Europe. Forest foliar Hg uptake fluxes generally follow a spatial distribution of European forests, because this map (Fig. 1) is based on the proportion of forest tree species per land area (Brus et al., 2012). Consequently, the largest forest foliage Hg uptake fluxes in terms of area are on the Scandinavian Peninsula with dense forest land cover. Outside of Scandinavia, forest foliage Hg uptake fluxes fall along large contiguous forested areas, e.g. in the Carpathian Mountains, the South-Eastern Alps, the Balkans, or forested low mountain areas like the Black Forest.

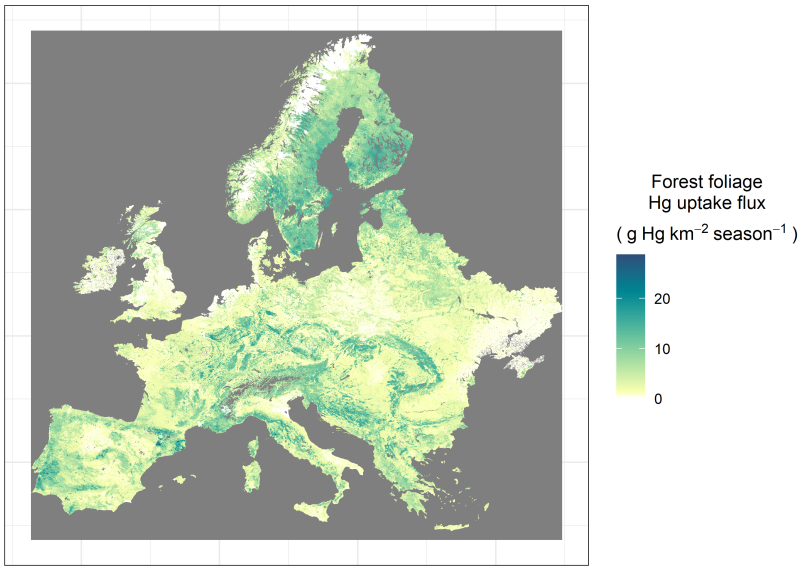

Figure 1. Spatial distribution of forest foliar Hg uptake fluxes (g Hg km^2 growing season^{-1}) to Europe based on a bottom-up extrapolation of foliar Hg concentrations, that were measured and averaged over the 2015 and 2017 growing seasons. Dark grey areas represent excluded non-forested areas (e.g. surface waters or non-vegetated mountain areas).

The sum of forest foliar Hg uptake fluxes over the land area of Europe as displayed in Figure 1 equals 23 ± 12 Mg Hg season^{-1}. This total flux agrees within uncertainty

with a previous estimate for the total foliar Hg uptake flux to Europe of 20 ± 3 Mg Hg over the 2018 growing season based on foliar Hg uptake fluxes at four forested sites (Wohlgemuth et al., 2020). (Zhou & Obrist, 2021) evaluated a median global foliar Hg assimilation of 28 Mg yr^{-1} for deciduous broadleaf forests and 61 Mg yr^{-1} for evergreen needleleaf forests by combining foliar Hg concentrations with annual net foliar biomass production data of the respective forest types. From these global assimilation estimates by (Zhou & Obrist, 2021), we calculated a total foliar Hg assimilation of 29 Mg yr^{-1} to the deciduous and coniferous forest land area of Europe (for details see SI, Text S1), which is slightly higher but still within the uncertainty of the 23 ± 12 Mg Hg $season^{-1}$ from this study. However, foliar Hg uptake fluxes based on net primary foliar biomass production by Zhou and Obrist, (2021) (Zhou & Obrist, 2021) does not correct for lower foliar Hg uptake rates by shade leaves and multiyear old needles (see Sect. 2.2) relative to sun leaves and younger needles (Wohlgemuth et al., 2020), likely resulting in a systematic over-estimation. We assume, that the different time reference (seasonal vs. annual) of the flux from this study (23 ± 12 Mg Hg $season^{-1}$) and the flux derived from Zhou and Obrist, (2021) (Zhou & Obrist, 2021) (29 Mg Hg yr^{-1}) only plays a minor role for explaining the difference between the two fluxes, since we expect a small net foliar biomass production in Europe in winter outside of the growing season.

3.2 Pine foliar Hg uptake fluxes under different VPD scenarios

Figure 2 shows total pine forest foliar Hg uptake fluxes to Europe calculated under different conditions of atmospheric surface-level water VPD during four past growing seasons (1994, 2003, 2015/2017, 2018) and simulated for the years 2068 - 2082 as an average of multiple climate model outputs (see Sect. 2.2) under two different climate change scenarios (RCP 4.5 and RCP 8.5). The leftmost bar (Fig. 2) represents a theoretical baseline pine needle Hg uptake flux in absence of VPD induced stomatal control (potential maximum transpiration rates) on the pine needle Hg uptake flux. The total pine needle Hg uptake flux to Europe during the reference growing season 2015/2017 (Sect. 2.2) is 9.3 ± 3.7 Mg Hg representing 70% of the baseline flux of 13.3 ± 5.3 Mg Hg $season^{-1}$. Thus, based on the pine needle Hg uptake model used in this study (Sect. 2.3), the VPD effect reduces the total pine needle Hg uptake flux to Europe by approximately 30%.

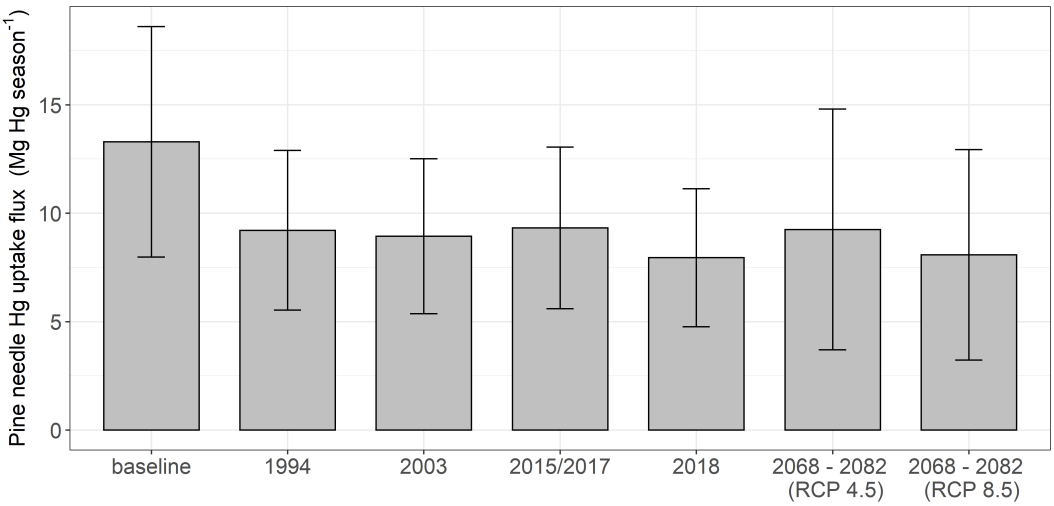

Figure 2. Pine needle Hg uptake flux to European pine forests (Mg Hg season^{-1}) calculated from atmospheric surface water vapor pressure deficit (VPD) conditions during the growing seasons 1994, 2003, 2015/2017, 2018 and projected for the years 2068 - 2082 under RCP 4.5 and RCP 8.5. Bar on the left represents a baseline pine forest needle Hg uptake flux with no VPD exceedance of 1.2 kPa throughout the growing season.

The relative standard deviation of modelled total pine needle Hg uptake fluxes for the investigated growing seasons (1994, 2003, 2015/2017, 2018, 2068 - 2082) was 0.07. Consequently, modelled total European pine needle Hg uptake fluxes hardly differed from each other among growing seasons. The total pine needle Hg uptake flux in Europe depend on VPD conditions in areas where pine forests prevail. Pine forests are primarily located in Northern Europe (SI Fig. 1), where hourly ambient VPD was > 1.2 kPa during 30% or less of daytime in the growing seasons 1994, 2003 and 2015/2017 due to relatively cool and moist ambient conditions as compared to Central and Southern Europe (see e.g. VPD conditions during reference time period 2015/2017 Fig. 3a). In contrast to previous years, the European summer hydrological condition of 2018 has been described as an intense hot drought, during which pronounced stomatal closure of coniferous forests in response to high VPD were recorded in Switzerland (Gharun et al., 2020). In Southern Fennoscandia, conditions of ambient hourly VPD > 1.2 kPa prevailed over exceptionally long time proportions (around 40%) during the summer of 2018 (see Fig. 3b, (Buras et al., 2020)). As a result, the modelled total pine needle Hg uptake flux in Europe in 2015/2017 (9.3 Mg Hg season^{-1}) was by a factor of 1.16 higher than the respective flux in 2018 (8.0 Mg Hg season^{-1}). We conclude that hot and dry summer conditions (Fig. 2) in Fennoscandia crucially impact modelled past total pine needle Hg uptake fluxes in Europe. According to the model results, an average amount of 1.3 Mg Hg was not deposited via pine needle uptake in 2018 compared to 2015/17, potentially remaining in the atmosphere, where it can be long-range transported to the ocean (Zhou et al., 2021). These 1.3 Mg Hg are more than three times larger than the reported anthropogenic Hg emissions of Sweden in 2021 **??**, highlighting the quantitative impact, that hot droughts can have on the pine needle Hg uptake flux.

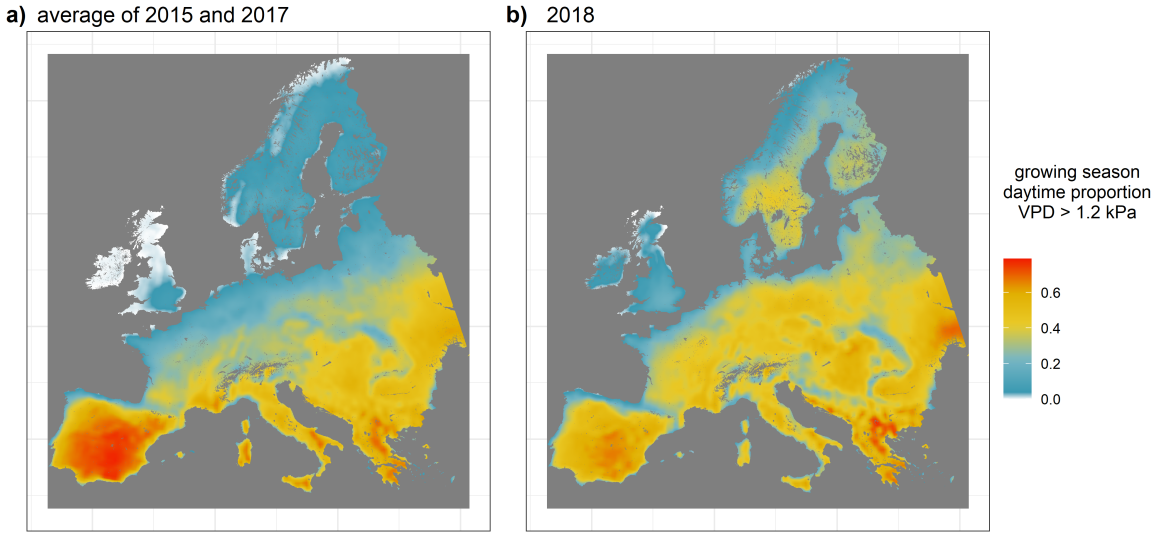

Figure 3. Average daytime proportion of surface level atmospheric water VPD > 1.2 kPa during a) the reference growing season 2015/2017, and b) the growing season 2018. All VPD values were calculated from hourly reanalysis data of ERA5 ambient air temperature and relative humidity (Sect. 2.1).

3.3 Projected pine forest needle Hg uptake fluxes under climate change scenarios

The projected total pine forest needle Hg uptake flux for 2068 - 2082 (RCP 4.5: 9.3 ± 5.5 Mg Hg season^{-1}; RCP 8.5: 8.1 ± 4.9 Mg Hg season^{-1}) was in the same range as the corresponding average flux for the years 1994, 2003, 2015 and 2017 of 9.1 ± 0.2 Mg Hg season^{-1} (mean ± sd), but slightly higher than the corresponding flux in the year of 2018 (8.0 ± 3.2 Mg Hg season^{-1}), during which Fennoscandia experienced a summer of relatively long hot and dry ambient conditions. Figure 4 maps the absolute deviation of the pine forest needle Hg uptake flux projected for 2068 - 2082 (simulated future flux) from the corresponding 2018 flux in Europe. Under RCP 4.5, the simulated future flux is higher (blue area in Fig. 4 a) than the 2018 flux in 65% of total area. Under RCP 8.5, the simulated future flux is higher (blue area in Fig. 4 b) than the 2018 flux in 43% of total area. In most area of Fennoscandia, where a majority of pine forests in Europe are located (SI Fig. 1a), the future flux is projected to be larger than in 2018. For both climate change scenarios, the projection predicts lower pine needle Hg fluxes to the Balkans and to the Southern Iberian Peninsula than in 2018 (Fig. 4).

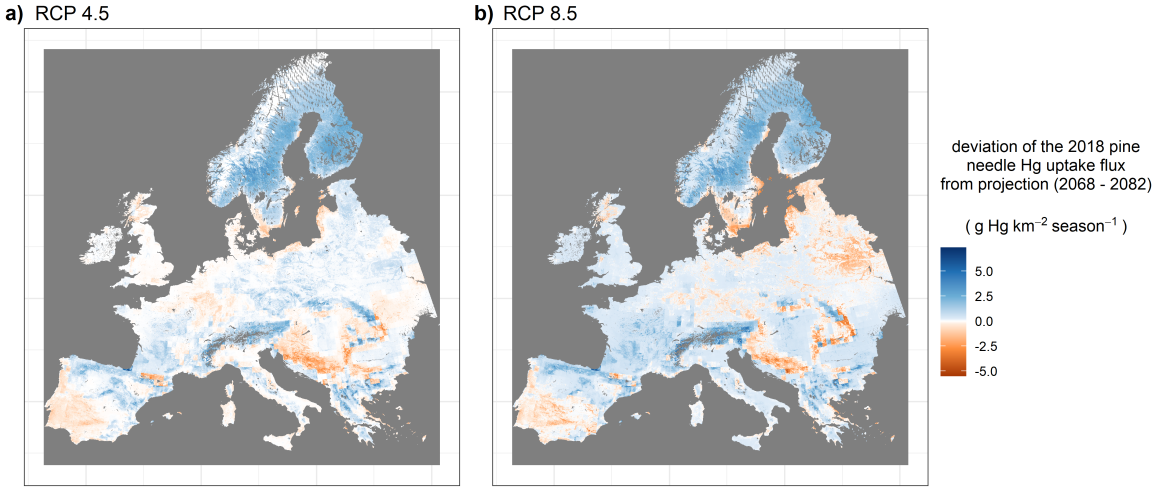

Figure 4. Absolute deviation of projected pine forest foliar Hg uptake fluxes for 2068 - 2082 (under RCP 4.5 (a) and RCP 8.5 (b)) from the corresponding flux modelled for 2018. In blue areas, the projected future flux under the two climate change scenarios is higher than the respective 2018 flux, in orange areas, this deviation is reversed.

The pine forest needle Hg uptake flux for 2068 - 2082 simulated here is a function of both modelled ambient VPD conditions during the growing season and the projected distribution of pine forests in Europe depending on climate analogs (Buras & Menzel, 2019). While the pine forest cover in Southern Sweden is projected to decrease under the climate change scenarios RCP 4.5 and RCP 8.5 from around 50% km^{-2} to around 25% km^{-2}, forest cover in Central and Northern Fennoscandia is projected to be relatively steady for climate analogs of both climate change scenarios (compare SI Fig. 1 a - c). Average long-term precipitation rates are projected to increase in Scandinavia, along with a decrease of meteorological drought in the coming decades under different climate change scenarios (Forzieri et al., 2014; Samaniego et al., 2018; Kellomäki et al., 2018), which could result in an increase of atmospheric humidity and a decrease of VPD in northern Europe (Oksanen et al., 2019). Under this scenario of wetter forest environments, the Hg sink of Scandinavian pine forest needles would not be significantly diminished. However, drought trends in Fennoscandia are still inconsistent and extreme drought events like in 2018 might occur more frequently under the current rate of climate change (IPCC, 2021a). The summer of 2018 was a record hot drought in Europe (Buras et al., 2020), while climate simulations for 2068 - 2082 are averaged over multiple climate models (SI Table 3), possibly averaging out extreme events. In a scenario, where the maximum proportion of daytime VPD $>$ 1.2 kPA per growing season averaged over 2068 - 2082 prevails at each spatial unit, the total pine forest needle Hg uptake flux to Europe reduces to 6.9 Mg Hg season^{-1} for RCP 4.5 and 5.0 Mg Hg season^{-1} for RCP 8.5, which corresponds to 74% and 62% of the respective flux derived from an average VPD daytime proportion. We therefore suggest that extreme climate events of extended time periods of ambient daytime VPD $>$ 1.2 kPa like during the growing season 2018 (Fig. 3b) could reduce the pine forest needle Hg uptake flux in Fennoscandia in future even compared to average long-term VPD projections (Fig. 4).

A source of model uncertainty of the future forest foliar Hg uptake flux under climate change arises from atmospheric Hg(0) concentrations that depend on anthropogenic emissions, re-emissions of mobilized legacy Hg and future global deposition fluxes under climate and land use change (Sonke et al., 2023; Feinberg et al., 2023), which we could not account for in this study. However, our model outputs call attention to the sensi-

tivity of the pine needle Hg uptake flux to extreme hot and dry ambient conditions, which should be accounted for in chemistry-transport models under varying atmospheric Hg(0) levels. The impact of the hot and dry conditions on the pine Hg uptake fluxes might have implications for Hg inputs into aquatic ecosystems. In a recent review on Hg cycling in the context of global change, (Sonke et al., 2023) highlighted the potential of legacy Hg (i.e. actively cycling Hg that was mobilized in the past) to cause contamination by mobilization of Hg from soils to wetlands and coastal ecosystems via riverine systems. While most soil Hg enters riverine systems by soil erosion from agricultural lands, contaminated sites, and deforested woodland (Panagos et al., 2021; Sonke et al., 2023), a reduced forest foliar Hg uptake and subsequent deposition to forest soils may decrease the amount of runoff Hg from forest soils in the long-term, while long-range Hg transport to the open ocean via the atmosphere might be enhanced (Zhou et al., 2021).

3.4 Comparison of bottom-up model with GEOS-Chem

Figure 5 depicts spatial ratios of daily forest Hg uptake fluxes of the bottom-up model to GEOS-Chem. Absolute difference values of the two model outputs are shown in SI Fig. 2.

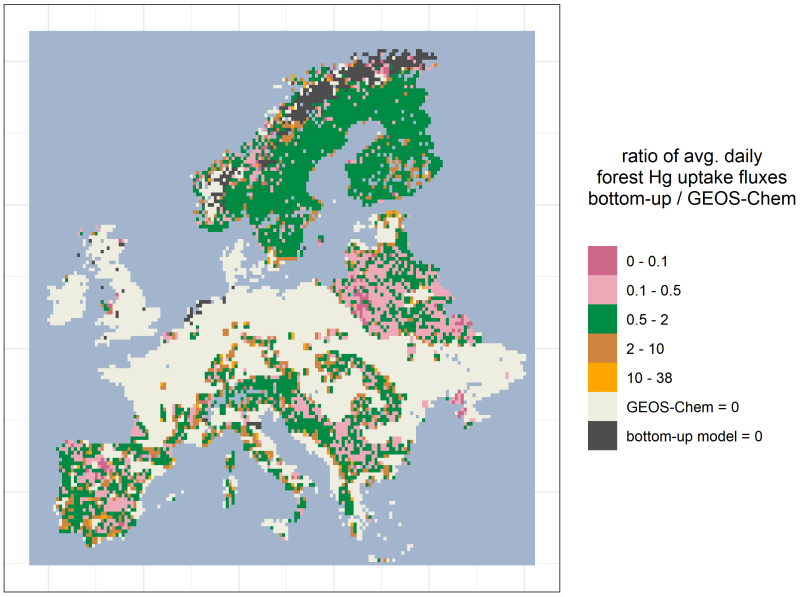

Figure 5. Ratios per spatial unit of daily forest Hg uptake fluxes averaged over the latitude-specific growing season length of the bottom-up model to GEOS-Chem.

Results of average daily foliar Hg uptake fluxes from GEOS-Chem and the bottom-up model were geographically comparable: In 59% of the spatial domain with values > 0, average daily foliar Hg uptake fluxes from the two models differed by factor of 1 - 2 from each other, in 37% of the domain, model values differed by a factor of 2 - 10 from each other, and in 4% of the domain respective values differed by a factor of > 10 from each other (Fig 5). We examined if differences in modelled average daily foliar Hg uptake fluxes at the same geographic location originate from differences in the underlying forest distribution maps of the two compared models. In 78% of spatial tiles with values > 0, the ratio of average daily foliar Hg uptake fluxes of the bottom-up model to GEOS-Chem agreed in range (Fig. 5) with the ratio of the forest fraction of the bottom-up model

to GEOS-Chem per respective spatial tile. We thus hypothesize that the bottom-up model and GEOS-Chem generally produce similar foliar Hg flux values per spatial unit given the same forest distribution. Reasons for minor differences in model outputs are challenging to identify, since the two models are based on different approaches, parameters and underlying maps (Sect. 2.4). For future assessment of model accuracy, we therefore suggest to compare model results to actual measurements of the forest foliar Hg uptake flux (Obrist et al., 2021; Feinberg et al., 2022). The total foliar Hg uptake flux to the European forested area (Fig. 1 and 5) was 22 Mg Hg season^{-1} for GEOS-Chem which almost equals the total flux of 23 $\pm$ 12 Mg Hg season^{-1} for the bottom-up model (Sect. 3.1).

4 Conclusion

We created a highly resolved (1 km^2) map (Fig. 1), which visualizes the spatial variation of foliar Hg uptake fluxes to European forests. The highest foliar Hg uptake fluxes receive Fennoscandia, densely forested areas in Central and Southern Europe , e.g. the Carpathian Mountains, the Balkans, or multiple low mountain areas. We suggest, that this map (Fig. 1) can guide decisions on European background Hg monitoring of the terrestrial environment. The total forest foliar Hg uptake flux over the course of one growing season agrees well with Hg flux estimates derived from literature and from the chemical transport model GEOS-Chem for the same land area of Europe (Fig. 5). This precision among modelling results on a European scale using different approaches gives us confidence that the bottom-up model is overall able to represent the seasonal forest foliar Hg uptake flux. We suggest that the accuracy of modelling results have to be further determined using direct forest foliar Hg flux measurements.

Using an empirical relationship between Hg needle uptake rates of pine trees and VPD threshold exceedance, we found a reduction in modelled pine forest needle Hg uptake flux during the relatively hot and dry growing season in Fennoscandia in 2018 compared to the growing seasons in 1994, 2003 and 2015/2017 (Fig. 2). The modelled average amount of Hg, that was not deposited via pine needle uptake in 2018 compared to the reference time period of 2015/17 exceeded the reported anthropogenic Hg emissions of Sweden in 2021, highlighting the quantitative significance of stomatal Hg uptake. If these hot summer droughts occurred more frequently in Fennoscandia under climate change, the pine forest needle Hg uptake flux would be diminished while these extreme conditions prevail, potentially increasing the Hg burden of the ocean via long-range atmospheric transport. In order to better represent the impact of extreme climate events on the pine forest needle Hg uptake flux, we therefore advise to incorporate a stomatal component of the pine needle Hg uptake flux into chemical transport models like GEOS-Chem.

5 Open Research

Calculated forest foliar Hg uptake fluxes to Europe (Fig. 1) and GEOS-Chem simulation data aggregated to seasonal values are publicly available for download from Zenodo at `https://zenodo.org/record/7851718#.ZFUeLM5Bw2w` and `https://zenodo.org/record/7900753#.ZFUgqM5Bw2w` respectively. All input datasets to the bottom-up model are described in detail in Section 2.1, along with their respective publications and databases, from which the datasets can be accessed. The offline dry deposition code from GEOS-Chem is accessible for download (Feinberg, 2022) and model output data from GEOS-Chem can be obtained from the corresponding author upon request. All calculations and visualizations were done in R, Version 4.0.3.

Acknowledgments

L. Wohlgemuth and M. Jiskra acknowledge financial support from the Swiss National Science Foundation (grant no. 174101). A. Feinberg acknowledges financial support from the Swiss National Science Foundation (Early Postdoc.Mobility grant: P2EZP2 195424) and the US National Science Foundation (#1924148). The GEOS-FP data used in this study/project have been provided by the Global Modeling and Assimilation Office (GMAO) at NASA Goddard Space Flight Center. The evaluation was partly based on data that was collected by partners of the official UNECE ICP Forests Network (http://icp-forests.net/contributors). Part of the ICP Forests data was co-financed by the European Commission. ERA5 and CORDEX data were obtained from the Copernicus Climate Change Service (C3S) Climate Data Store (https://cds.climate.copernicus.eu/cdsapp#!/home). PROBA-V leaf area index values were downloaded from the VITO Product Distribution Portal. Climate calculations under two climate change scenarios (Fig. 2, Fig. 3) were performed at sciCORE (http://scicore.unibas.ch/) scientific computing center at University of Basel.

References

Allen, C. D., Breshears, D. D., & McDowell, N. G. (2015). On underestimation of global vulnerability to tree mortality and forest die-off from hotter drought in the Anthropocene. *Ecosphere*, *6*(8), art129. Retrieved 2021-10-22, from `https://onlinelibrary.wiley.com/doi/abs/10.1890/ES15-00203.1` doi: 10.1890/ES15-00203.1

Berg, A., & Sheffield, J. (2018, June). Climate Change and Drought: the Soil Moisture Perspective. *Curr Clim Change Rep*, *4*(2), 180–191. Retrieved 2021-10-22, from `https://doi.org/10.1007/s40641-018-0095-0` doi: 10.1007/s40641-018-0095-0

Blackwell, B. D., Driscoll, C. T., Maxwell, J. A., & Holsen, T. M. (2014, June). Changing climate alters inputs and pathways of mercury deposition to forested ecosystems. *Biogeochemistry*, *119*(1-3), 215–228. Retrieved 2020-03-10, from `http://link.springer.com/10.1007/s10533-014-9961-6` doi: 10.1007/s10533-014-9961-6

Brando, P. M., Paolucci, L., Ummenhofer, C. C., Ordway, E. M., Hartmann, H., Cattau, M. E., ... Balch, J. (2019, May). Droughts, Wildfires, and Forest Carbon Cycling: A Pantropical Synthesis. *Annu. Rev. Earth Planet. Sci.*, *47*(1), 555–581. Retrieved 2021-10-22, from `https://www.annualreviews.org/doi/10.1146/annurev-earth-082517-010235` doi: 10.1146/annurev-earth-082517-010235

Brus, D. J., Hengeveld, G. M., Walvoort, D. J. J., Goedhart, P. W., Heidema, A. H., Nabuurs, G. J., & Gunia, K. (2012, January). Statistical mapping of tree species over Europe. *European Journal of Forest Research*, *131*(1), 145–157. Retrieved 2019-08-26, from `http://link.springer.com/10.1007/s10342-011-0513-5` doi: 10.1007/s10342-011-0513-5

Buras, A., & Menzel, A. (2019). Projecting Tree Species Composition Changes of European Forests for 2061–2090 Under RCP 4.5 and RCP 8.5 Scenarios. *Frontiers in Plant Science*, *9*, 1986. Retrieved 2021-09-22, from `https://www.frontiersin.org/article/10.3389/fpls.2018.01986` doi: 10.3389/fpls.2018.01986

Buras, A., Rammig, A., & Zang, C. S. (2020, March). Quantifying impacts of the 2018 drought on European ecosystems in comparison to 2003. *Biogeosciences*, *17*(6), 1655–1672. Retrieved 2021-12-07, from `https://bg.copernicus.org/articles/17/1655/2020/` doi: 10.5194/bg-17-1655-2020

C3S. (2022). Copernicus Climate Change Service, Climate Data Store (CDS): CORDEX regional climate model data on single levels. Retrieved from `https://cds.climate.copernicus.eu/cdsapp#!/dataset/10.24381/cds.bc91edc3?tab=overview` doi: 10.24381/cds.bc91edc3

CLRTAP. (2017). Revised Chapter 3 of the Manual on Methodologies and Criteria for Modelling and Mapping Critical Loads and Levels and Air Pollution Effects, Risks and Trends: Mapping Critical Levels for Vegetation. *Umweltbundesamt*. Retrieved from https://www.umweltbundesamt.de/en/manual-for-modelling-mapping-critical-loads-levels doi: https://www.umweltbundesamt.de/en/manual-for-modelling-mapping-critical-loads-levels

Demers, J. D., Blum, J. D., & Zak, D. R. (2013, March). Mercury isotopes in a forested ecosystem: Implications for air-surface exchange dynamics and the global mercury cycle. *Global Biochem. Cy.*, *27*(1), 222–238. Retrieved 2018-11-14, from https://agupubs.onlinelibrary.wiley.com/doi/abs/10.1002/gbc.20021 doi: 10.1002/gbc.20021

Dierckx, W., Sterckx, S., Benhadj, I., Livens, S., Duhoux, G., Van Achteren, T., ... Saint, G. (2014, April). PROBA-V mission for global vegetation monitoring: standard products and image quality. *Int. J. Remote Sens.*, *35*(7), 2589–2614. Retrieved 2021-08-30, from https://doi.org/10.1080/01431161.2014.883097 doi: 10.1080/01431161.2014.883097

Enrico, M., Roux, G. L., Marusczak, N., Heimbürger, L.-E., Claustres, A., Fu, X., ... Sonke, J. E. (2016, March). Atmospheric mercury transfer to peat bogs dominated by gaseous elemental mercury dry deposition. *Environ. Sci. Technol.*, *50*(5), 2405–2412. Retrieved 2019-06-20, from http://pubs.acs.org/doi/10.1021/acs.est.5b06058 doi: 10.1021/acs.est.5b06058

Feinberg, A. (2022). Code reference: arifein/offline-drydep: Offline dry deposition model from GEOS-Chem v1.0 (v1.0). doi: https://doi.org/10.5281/zenodo.6498126

Feinberg, A., Dlamini, T., Jiskra, M., Shah, V., & E. Selin, N. (2022). Evaluating atmospheric mercury (Hg) uptake by vegetation in a chemistry-transport model. *Environmental Science: Processes & Impacts*. Retrieved 2022-07-25, from https://pubs.rsc.org/en/content/articlelanding/2022/em/d2em00032f (Publisher: Royal Society of Chemistry) doi: 10.1039/D2EM00032F

Feinberg, A., Jiskra, M., Borrelli, P., Biswakarma, J., & Selin, N. E. (2023, January). Land use change as an anthropogenic driver of mercury pollution. Retrieved 2023-04-15, from https://eartharxiv.org/repository/view/4963/ (Publisher: EarthArXiv)

Forrester, D. I., Tachauer, I. H. H., Annighoefer, P., Barbeito, I., Pretzsch, H., Ruiz-Peinado, R., ... Sileshi, G. W. (2017, July). Generalized biomass and leaf area allometric equations for European tree species incorporating stand structure, tree age and climate. *Forest Ecology and Management*, *396*, 160–175. Retrieved 2020-06-10, from http://www.sciencedirect.com/science/article/pii/S0378112717301238 doi: 10.1016/j.foreco.2017.04.011

Forzieri, G., Feyen, L., Rojas, R., Flörke, M., Wimmer, F., & Bianchi, A. (2014, January). Ensemble projections of future streamflow droughts in Europe. *Hydrology and Earth System Sciences*, *18*(1), 85–108. Retrieved 2021-12-17, from https://hess.copernicus.org/articles/18/85/2014/ (Publisher: Copernicus GmbH) doi: 10.5194/hess-18-85-2014

Fuster, B., Sánchez-Zapero, J., Camacho, F., García-Santos, V., Verger, A., Lacaze, R., ... Smets, B. (2020, January). Quality assessment of PROBA-V LAI, fAPAR and fCOVER collection 300 m products of Copernicus Global Land Service. *Remote Sens.*, *12*(6), 1017. Retrieved 2021-03-17, from https://www.mdpi.com/2072-4292/12/6/1017 doi: 10.3390/rs12061017

Garonna, I., Jong, R. d., Wit, A. J. W. d., Mücher, C. A., Schmid, B., & Schaepman, M. E. (2014). Strong contribution of autumn phenology to changes in satellite-derived growing season length estimates across Europe (1982–2011). *Glob. Change Biol.*, *20*(11), 3457–3470. Retrieved 2019-10-17, from https://onlinelibrary.wiley.com/doi/abs/10.1111/gcb.12625 doi:

10.1111/gcb.12625

Gharun, M., Hörtnagl, L., Paul-Limoges, E., Ghiasi, S., Feigenwinter, I., Burri, S., ... Buchmann, N. (2020, September). Physiological response of Swiss ecosystems to 2018 drought across plant types and elevation. *Philosophical Transactions of the Royal Society B: Biological Sciences*, *375*(1810), 20190521. Retrieved 2023-04-16, from `https://royalsocietypublishing.org/doi/full/10.1098/rstb.2019.0521` (Publisher: Royal Society) doi: 10.1098/rstb.2019.0521

Gibbs, H. K. (2006). Olson's Major World Ecosystem Complexes Ranked by Carbon in Live Vegetation: an Updated Database Using the GLC2000 Land Cover Product (NDP-017b).
doi: https://www.osti.gov/biblio/1389498

Grossiord, C., Buckley, T. N., Cernusak, L. A., Novick, K. A., Poulter, B., Siegwolf, R. T. W., ... McDowell, N. G. (2020). Plant responses to rising vapor pressure deficit. *New Phytol.*, *226*(6), 1550–1566. Retrieved 2020-09-07, from `https://nph.onlinelibrary.wiley.com/doi/abs/10.1111/nph.16485` doi: 10.1111/nph.16485

Hararuk, O., Obrist, D., & Luo, Y. (2013, April). Modelling the sensitivity of soil mercury storage to climate-induced changes in soil carbon pools. *Biogeosciences*, *10*(4), 2393–2407. Retrieved 2021-10-27, from `https://bg.copernicus.org/articles/10/2393/2013/` doi: 10.5194/bg-10-2393-2013

Hersbach, H., Bell, B., Berrisford, P., Biavati, G., Horányi, A., Muñoz Sabater, J., ... Thépaut, J.-N. (2018). ERA5 hourly data on pressure levels from 1979 to present. Copernicus Climate Change Service (C3S) Climate Data Store (CDS).
doi: 10.24381/cds.bd0915c6

IPCC. (2021a). Climate change 2021. The physical science basis. Working group I contribution to the Sixth Assessment Report of the Intergovernmental Panel on Climate Change.

IPCC. (2021b). Summary for Policymakers. Climate Change 2021: The Physical Science Basis. Contribution of Working Group I to the Sixth Assessment Report of the Intergovernmental Panel on Climate Change. , *Cambride University Press*.

Jacob, D., Teichmann, C., Sobolowski, S., Katragkou, E., Anders, I., Belda, M., ... Wulfmeyer, V. (2020, April). Regional climate downscaling over Europe: perspectives from the EURO-CORDEX community. *Reg Environ Change*, *20*(2), 51. Retrieved 2021-11-03, from `https://doi.org/10.1007/s10113-020-01606-9` doi: 10.1007/s10113-020-01606-9

Jeong, S.-J., Ho, C.-H., Gim, H.-J., & Brown, M. E. (2011). Phenology shifts at start vs. end of growing season in temperate vegetation over the Northern Hemisphere for the period 1982–2008. *Global Change Biology*, *17*(7), 2385–2399. Retrieved 2021-12-20, from `https://onlinelibrary.wiley.com/doi/abs/10.1111/j.1365-2486.2011.02397.x` doi: 10.1111/j.1365-2486.2011.02397.x

Jiskra, M., Sonke, J. E., Obrist, D., Bieser, J., Ebinghaus, R., Myhre, C. L., ... Dommergue, A. (2018). A vegetation control on seasonal variations in global atmospheric mercury concentrations. *Nat. Geosci.*, 1–7. Retrieved from `http:https://doi.org/10.1038/s41561-018-0078-8` doi: 10.1038/s41561-018-0078-8

Jiskra, M., Wiederhold, J. G., Skyllberg, U., Kronberg, R.-M., Hajdas, I., & Kretzschmar, R. (2015). Mercury deposition and re-emission pathways in boreal forest soils investigated with Hg isotope signatures. *Environ. Sci. Technol.*, *49*(12), 7188–7196.

Kellomäki, S., Strandman, H., Heinonen, T., Asikainen, A., Venäläinen, A., & Peltola, H. (2018, March). Temporal and Spatial Change in Diameter Growth

of Boreal Scots Pine, Norway Spruce, and Birch under Recent-Generation (CMIP5) Global Climate Model Projections for the 21st Century. *Forests*, *9*(3), 118. Retrieved 2021-12-16, from https://www.mdpi.com/1999-4907/9/3/118 doi: 10.3390/f9030118

Khan, T., Obrist, D., Agnan, Y., E. Selin, N., & A. Perlinger, J. (2019). Atmosphere-terrestrial exchange of gaseous elemental mercury: parameterization improvement through direct comparison with measured ecosystem fluxes. *Environmental Science: Processes & Impacts*, *21*(10), 1699–1712. Retrieved 2021-10-20, from https://pubs.rsc.org/en/content/articlelanding/2019/em/c9em00341j doi: 10.1039/C9EM00341J

Ku, H. (1966). Notes on the use of propagation of error formulas. *Journal of Research of the National Bureau of Standards*, *70C*(4).

Körner, C. (2013). Plant–Environment Interactions. In A. Bresinsky, C. Körner, J. W. Kadereit, G. Neuhaus, & U. Sonnewald (Eds.), *Strasburger's Plant Sciences: Including Prokaryotes and Fungi* (pp. 1065–1166). Berlin, Heidelberg: Springer. Retrieved 2019-11-25, from https://doi.org/10.1007/978-3-642-15518-5_12

Laacouri, A., Nater, E. A., & Kolka, R. K. (2013, September). Distribution and uptake dynamics of mercury in leaves of common deciduous tree species in Minnesota, U.S.A. *Environ. Sci. Technol.*, *47*(18), 10462–10470. Retrieved 2019-06-20, from http://pubs.acs.org/doi/abs/10.1021/es401357z doi: 10.1021/es401357z

Lagergren, F., & Lindroth, A. (2002, August). Transpiration response to soil moisture in pine and spruce trees in Sweden. *Agr. Forest Meteorol.*, *112*(2), 67–85. Retrieved 2021-08-31, from https://www.sciencedirect.com/science/article/pii/S0168192302000606 doi: 10.1016/S0168-1923(02)00060-6

Liu, Y., Liu, G., Wang, Z., Guo, Y., Yin, Y., Zhang, X., ... Jiang, G. (2021, October). Understanding foliar accumulation of atmospheric Hg in terrestrial vegetation: Progress and challenges. *Critical Reviews in Environmental Science and Technology*, *0*(0), 1–22. Retrieved 2021-10-18, from https://doi.org/10.1080/10643389.2021.1989235 doi: 10.1080/10643389.2021.1989235

Lucchesi, R. (2018). File Specification for GEOS FP. GMAO Office Note No. 4 (Version 1.2). Retrieved from http://gmao.gsfc.nasa.gov/pubs/office_notes

Mauri, A., Strona, G., & San-Miguel-Ayanz, J. (2017, January). EU-Forest, a high-resolution tree occurrence dataset for Europe. *Sci Data*, *4*. Retrieved 2020-01-29, from https://www.ncbi.nlm.nih.gov/pmc/articles/PMC5215058/ doi: 10.1038/sdata.2016.123

Norby, R. J., & Zak, D. R. (2011). Ecological Lessons from Free-Air CO2 Enrichment (FACE) Experiments. *Annual Review of Ecology, Evolution, and Systematics*, *42*(1), 181–203. Retrieved 2021-10-22, from https://doi.org/10.1146/annurev-ecolsys-102209-144647 doi: 10.1146/annurev-ecolsys-102209-144647

Obrist, D., Agnan, Y., Jiskra, M., Olson, C. L., Colegrove, D. P., Hueber, J., ... Helmig, D. (2017, July). Tundra uptake of atmospheric elemental mercury drives Arctic mercury pollution. *Nature*, *547*(7662), 201–204. Retrieved 2019-06-24, from http://www.nature.com/articles/nature22997 doi: 10.1038/nature22997

Obrist, D., Roy, E. M., Harrison, J. L., Kwong, C. F., Munger, J. W., Moosmüller, H., ... Commane, R. (2021, July). Previously unaccounted atmospheric mercury deposition in a midlatitude deciduous forest. *PNAS*, *118*(29). Retrieved 2021-07-26, from https://www.pnas.org/content/118/29/e2105477118 doi: 10.1073/pnas.2105477118

Oksanen, E., Lihavainen, J., Keinänen, M., Keski-Saari, S., Kontunen-Soppela, S., Sellin, A., & Sõber, A. (2019). Northern Forest Trees Under Increasing Atmospheric Humidity. In F. M. Cánovas, U. Lüttge, R. Matyssek, & H. Pretzsch

(Eds.), *Progress in Botany Vol. 80* (pp. 317–336). Cham: Springer International Publishing. Retrieved 2021-12-17, from https://doi.org/10.1007/124_2017_15

Pan, Y., Birdsey, R. A., Phillips, O. L., & Jackson, R. B. (2013, November). The Structure, Distribution, and Biomass of the World's Forests. *Annu. Rev. Ecol. Evol. Syst.*, *44*(1), 593–622. Retrieved 2022-01-10, from https://www.annualreviews.org/doi/10.1146/annurev-ecolsys-110512-135914 doi: 10.1146/annurev-ecolsys-110512-135914

Panagos, P., Jiskra, M., Borrelli, P., Liakos, L., & Ballabio, C. (2021, October). Mercury in European topsoils: Anthropogenic sources, stocks and fluxes. *Environmental Research*, *201*, 111556. Retrieved 2021-07-29, from https://www.sciencedirect.com/science/article/pii/S0013935121008501 doi: 10.1016/j.envres.2021.111556

Panek, J. A., & Goldstein, A. H. (2001, March). Response of stomatal conductance to drought in ponderosa pine: implications for carbon and ozone uptake. *Tree Physiol.*, *21*(5), 337–344. Retrieved 2021-07-22, from https://doi.org/10.1093/treephys/21.5.337 doi: 10.1093/treephys/21.5.337

Papula, L. (2003). *Mathematische Formelsammlung für Ingenieure und Naturwissenschaftler* (8th ed.). Vieweg.

Pleijel, H., Klingberg, J., Nerentorp, M., Broberg, M. C., Nyirambangutse, B., Munthe, J., & Wallin, G. (2021, December). Mercury accumulation in leaves of different plant types – the significance of tissue age and specific leaf area. *Biogeosciences*, *18*(23), 6313–6328. Retrieved 2021-12-23, from https://bg.copernicus.org/articles/18/6313/2021/ doi: 10.5194/bg-18-6313-2021

Rea, A. W., Lindberg, S. E., Scherbatskoy, T., & Keeler, G. J. (2002). Mercury accumulation in foliage over time in two northern mixed-hardwood forests. *Water Air Soil Poll.*, *133*, 49–67.

Rutter, A. P., Schauer, J. J., Shafer, M. M., Creswell, J. E., Olson, M. R., Robinson, M., ... Mallek, J. L. (2011, February). Dry deposition of gaseous elemental mercury to plants and soils using mercury stable isotopes in a controlled environment. *Atmos. Environ.*, *45*(4), 848–855. Retrieved 2019-09-24, from http://www.sciencedirect.com/science/article/pii/S1352231010009805 doi: 10.1016/j.atmosenv.2010.11.025

Samaniego, L., Thober, S., Kumar, R., Wanders, N., Rakovec, O., Pan, M., ... Marx, A. (2018, May). Anthropogenic warming exacerbates European soil moisture droughts. *Nature Clim Change*, *8*(5), 421–426. Retrieved 2021-12-17, from https://www.nature.com/articles/s41558-018-0138-5 doi: 10.1038/s41558-018-0138-5

Selin, N. E., Jacob, D. J., Yantosca, R. M., Strode, S., Jaeglé, L., & Sunderland, E. M. (2008). Global 3-D land-ocean-atmosphere model for mercury: Present-day versus preindustrial cycles and anthropogenic enrichment factors for deposition. *Global Biogeochemical Cycles*, *22*(2). Retrieved 2020-09-22, from https://agupubs.onlinelibrary.wiley.com/doi/abs/10.1029/2007GB003040 doi: 10.1029/2007GB003040

Smith-Downey, N. V., Sunderland, E. M., & Jacob, D. J. (2010). Anthropogenic impacts on global storage and emissions of mercury from terrestrial soils: Insights from a new global model. *Journal of Geophysical Research: Biogeosciences*, *115*(G3). Retrieved 2019-06-20, from https://agupubs.onlinelibrary.wiley.com/doi/abs/10.1029/2009JG001124 doi: 10.1029/2009JG001124

Sonke, J. E., Angot, H., Zhang, Y., Poulain, A., Björn, E., & Schartup, A. (2023, May). Global change effects on biogeochemical mercury cycling. *Ambio*, *52*(5), 853–876. Retrieved 2023-04-15, from https://doi.org/10.1007/s13280-023-01855-y doi: 10.1007/s13280-023-01855-y

Stocker, B. D., Zscheischler, J., Keenan, T. F., Prentice, I. C., Seneviratne, S. I., & Peñuelas, J. (2019, April). Drought impacts on terrestrial primary production underestimated by satellite monitoring. *Nat. Geosci.*, *12*(4), 264–270. Retrieved 2021-10-22, from https://www.nature.com/articles/s41561-019-0318-6 doi: 10.1038/s41561-019-0318-6

Wang, Q., Tenhunen, J., Dinh, N., Reichstein, M., Otieno, D., Granier, A., & Pilegarrd, K. (2005, June). Evaluation of seasonal variation of MODIS derived leaf area index at two European deciduous broadleaf forest sites. *Remote Sensing of Environment*, *96*(3-4), 475–484. Retrieved 2019-05-15, from https://linkinghub.elsevier.com/retrieve/pii/S0034425705001252 doi: 10.1016/j.rse.2005.04.003

Wang, R., Chen, J. M., Liu, Z., & Arain, A. (2017, August). Evaluation of seasonal variations of remotely sensed leaf area index over five evergreen coniferous forests. *ISPRS Journal of Photogrammetry and Remote Sensing*, *130*, 187–201. Retrieved 2020-10-13, from http://www.sciencedirect.com/science/article/pii/S0924271616305998 doi: 10.1016/j.isprsjprs.2017.05.017

Wang, Y., Jacob, D. J., & Logan, J. A. (1998). Global simulation of tropospheric O3-NO x -hydrocarbon chemistry: 1. Model formulation. *Journal of Geophysical Research: Atmospheres*, *103*(D9), 10713–10725. Retrieved 2022-05-25, from https://onlinelibrary.wiley.com/doi/abs/10.1029/98JD00158 (_eprint: https://onlinelibrary.wiley.com/doi/pdf/10.1029/98JD00158) doi: 10.1029/98JD00158

Wesely, M. L. (2007, January). Parameterization of surface resistances to gaseous dry deposition in regional-scale numerical models. *Atmospheric Environment*, *41*, 52–63. Retrieved 2021-10-21, from https://www.sciencedirect.com/science/article/pii/S1352231007009740 doi: 10.1016/j.atmosenv.2007.10.058

Wohlgemuth, L., Osterwalder, S., Joseph, C., Kahmen, A., Hoch, G., Alewell, C., & Jiskra, M. (2020, December). A bottom-up quantification of foliar mercury uptake fluxes across Europe. *Biogeosciences*, *17*(24), 6441–6456. Retrieved 2021-01-14, from https://bg.copernicus.org/articles/17/6441/2020/ doi: https://doi.org/10.5194/bg-17-6441-2020

Wohlgemuth, L., Rautio, P., Ahrends, B., Russ, A., Vesterdal, L., Waldner, P., ... Jiskra, M. (2022, March). Physiological and climate controls on foliar mercury uptake by European tree species. *Biogeosciences*, *19*(5), 1335–1353. Retrieved 2022-03-14, from https://bg.copernicus.org/articles/19/1335/2022/ (Publisher: Copernicus GmbH) doi: 10.5194/bg-19-1335-2022

Wu, Z., Wang, X., Chen, F., Turnipseed, A. A., Guenther, A. B., Niyogi, D., ... Alapaty, K. (2011, May). Evaluating the calculated dry deposition velocities of reactive nitrogen oxides and ozone from two community models over a temperate deciduous forest. *Atmospheric Environment*, *45*(16), 2663–2674. Retrieved 2021-10-21, from https://www.sciencedirect.com/science/article/pii/S1352231011002275 doi: 10.1016/j.atmosenv.2011.02.063

Yuan, H., Dai, Y., Xiao, Z., Ji, D., & Shangguan, W. (2011, May). Reprocessing the MODIS Leaf Area Index products for land surface and climate modelling. *Remote Sensing of Environment*, *115*(5), 1171–1187. Retrieved 2023-04-16, from https://www.sciencedirect.com/science/article/pii/S0034425711000149 doi: 10.1016/j.rse.2011.01.001

Yuan, W., Sommar, J., Lin, C.-J., Wang, X., Li, K., Liu, Y., ... Feng, X. (2019, January). Stable isotope evidence shows re-emission of elemental mercury vapor occurring after reductive loss from foliage. *Environ. Sci. Technol.*, *53*(2), 651–660. Retrieved 2019-11-29, from https://doi.org/10.1021/acs.est.8b04865 doi: 10.1021/acs.est.8b04865

Yuan, W., Zheng, Y., Piao, S., Ciais, P., Lombardozzi, D., Wang, Y., ... Yang, S. (2019, August). Increased atmospheric vapor pressure deficit re-

duces global vegetation growth. *Sci. Adv.*, *5*(8). Retrieved 2019-09-06, from https://advances.sciencemag.org/content/5/8/eaax1396 doi: 10.1126/sciadv.aax1396

Zhang, H., Holmes, C., & Wu, S. (2016, September). Impacts of changes in climate, land use and land cover on atmospheric mercury. *Atmospheric Environment*, *141*, 230–244. Retrieved 2021-10-21, from https://linkinghub.elsevier.com/retrieve/pii/S1352231016304897 doi: 10.1016/j.atmosenv.2016.06.056

Zhang, L., Wright, L. P., & Blanchard, P. (2009, December). A review of current knowledge concerning dry deposition of atmospheric mercury. *Atmos. Environ.*, *43*(37), 5853–5864. Retrieved 2019-10-03, from http://www.sciencedirect.com/science/article/pii/S1352231009007407 doi: 10.1016/j.atmosenv.2009.08.019

Zhou, J., & Obrist, D. (2021). Global mercury assimilation by vegetation. *Environ. Sci. Technol.*. Retrieved 2021-10-08, from https://doi.org/10.1021/acs.est.1c03530 doi: 10.1021/acs.est.1c03530

Zhou, J., Obrist, D., Dastoor, A., Jiskra, M., & Ryjkov, A. (2021, March). Vegetation uptake of mercury and impacts on global cycling. *Nat. Rev. Earth Environ.*, 1–16. Retrieved 2021-03-16, from https://www.nature.com/articles/s43017-021-00146-y doi: 10.1038/s43017-021-00146-y

Zweifel, R., Rigling, A., & Dobbertin, M. (2009). Species-specific stomatal response of trees to drought – a link to vegetation dynamics? *J. Veg. Sci.*, *20*(3), 442–454. Retrieved 2021-09-08, from https://onlinelibrary.wiley.com/doi/abs/10.1111/j.1654-1103.2009.05701.x doi: 10.1111/j.1654-1103.2009.05701.x

Zweifel, R., Steppe, K., & Sterck, F. J. (2007, June). Stomatal regulation by microclimate and tree water relations: interpreting ecophysiological field data with a hydraulic plant model. *J. Exp. Bot.*, *58*(8), 2113–2131. Retrieved 2021-04-19, from https://doi.org/10.1093/jxb/erm050 doi: 10.1093/jxb/erm050

Supporting Information for "A spatial assessment of current and future foliar Hg uptake fluxes across European forests"

Lena Wohlgemuth[1,2], Aryeh Feinberg[3], Allan Buras[4], Martin Jiskra[1]

[1]Department of Environmental Geosciences, University of Basel, Basel, Switzerland

[2]Thünen Institute of Forest Ecosystems, Eberswalde, Germany

[3]Institute for Data, Systems, and Society, MIT, Cambridge, USA

[4]TUM School of Life Sciences, Technical University of Munich, Munich, Germany

Contents of this file

Text S1.

Zhou & Obrist, (2021) give an estimate of median global foliage Hg assimilation by evergreen needleleaf forests of 61 Mg Hg year^{-1} and by deciduous broadleaf forests of 28 Mg Hg year^{-1} (Zhou & Obrist, 2021, Table 1). This estimate is based on global data on foliar Hg concentrations and net foliar biomass production. The global land area of evergreen needleleaf forests is given as 6.17 Mio km^2 and of deciduous broadleaf forests as 1.12 Mio km^2 (Zhou & Obrist, 2021). Converted to the land area of coniferous (1.0 Mio

km^2) and deciduous forests (0.73 Mio km^2) in Europe, we obtain a total Hg assimilation of 10.2 Mg Hg $year^{-1}$ for European coniferous forests and of 18.4 Mg Hg $year^{-1}$ for European deciduous forests.

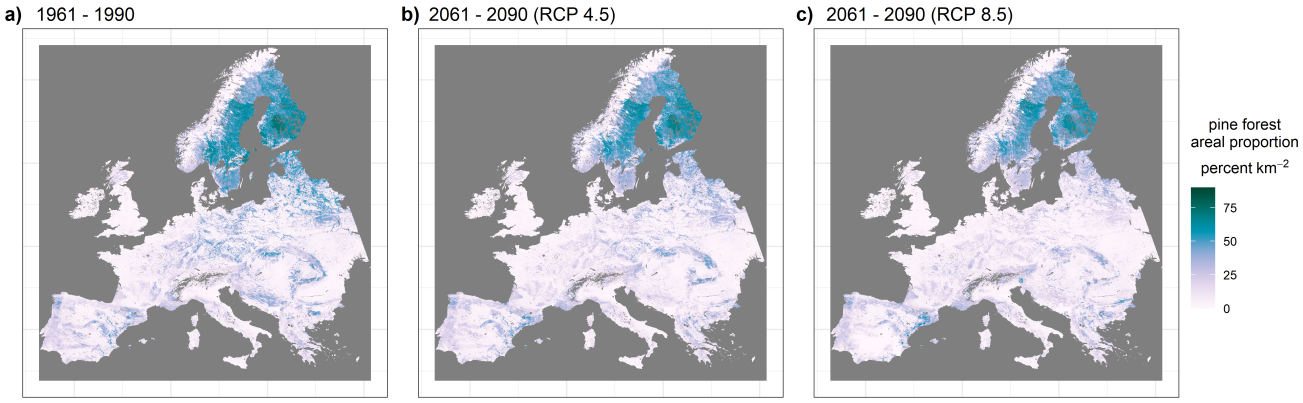

Figure S1. Simulated areal cover (percent km^{-2}) of pine forests in Europe (a) historically, (b) for the time period 2061 - 2090 under the climate change scenario RCP 4.5, and (c) RCP 8.5. Geographic distribution was derived from statistic mapping from Brus et al. 2012 and projected relative abundance probabilities under climate analogs from Buras et al. 2019 (see Sect. 2.1 for details).

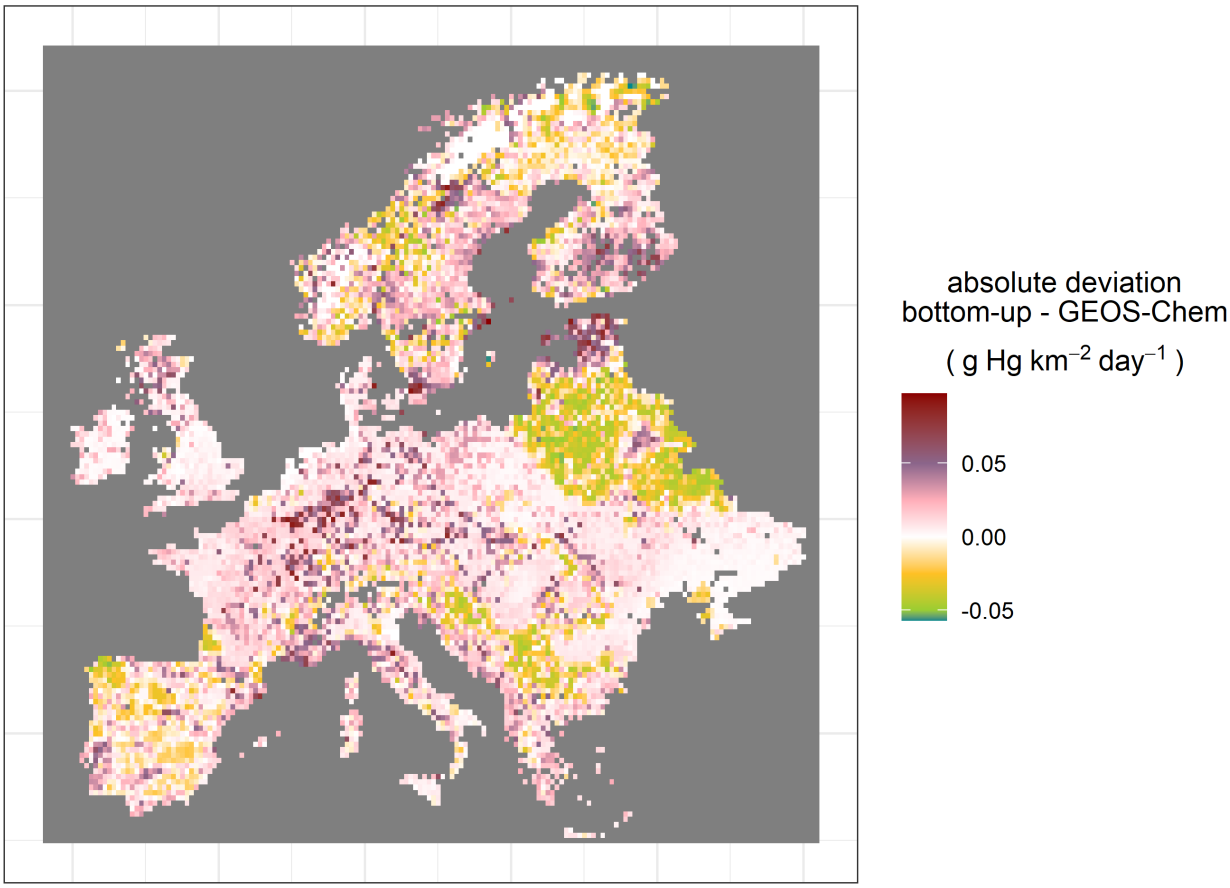

Figure S2. Absolute difference map of model outputs of forest foliar Hg uptake fluxes (g Hg km^{-2} day^{-1}) from the bottom-up model - GEOS-Chem.

Table S1. Overview of LAI correction factor for tree height (cf_{height}) and Hg uptake rate correction factor for needle age class (cf_{age}) obtained from Wohlgemuth et al., (2020).

Tree species group	$\mathbf{cf}_{height}$	$\mathbf{cf}_{age}$
Abies alba	0.68	0.79
mix of all broadleaf values	0.63	-
Betula pendula	0.63	-
Carpinus betulus	0.63	-
mix of all conifer values	0.68	0.79
Fagus sylvatica	0.56	-
Fraxinus excelsior	0.63	-
Larix decidua	0.68	-
Pinus cembra; *Pinus mugo arborea*; *Pinus nigra* *Pinus nigra subsp. laricio*	0.68	0.86
Picea abies	0.68	0.79
Pinus pinaster	0.68	0.86
Pinus sylvestris	0.68	0.86
Pinus sylvestris	0.68	0.86
Pseudotsuga menziesii	0.68	0.86
Quercus cerris; *Quercus frainetto*; *Quercus ilex*; *Quercus pubescens*	0.7	-
Quercus robur; *Quercus petraea*	0.7	-

Table S2. Dataset on proportion of tree species per land area matched to dataset on foliar Hg uptake rates by tree species groups.

Matched and aggregated tree species groups	
Dataset on tree species proportion of land area (Brus et al., 2012)	**Dataset on foliar Hg up–take per tree species (Wohlgemuth et al., 2022)**
Abies spp	*Abies alba*
Alnus spp; Broadleaved misc; Castanea spp; Eucalyptus spp; Populus spp; Robinia Spp	mix of all broadleaf values
Betula spp	*Betula pendula*
Carpinus spp	*Carpinus betulus*
Conifers misc	mix of all conifer values
Fagus spp	*Fagus sylvatica*
Fraxinus spp	*Fraxinus excelsior*
Larix spp	*Larix decidua*
Picea spp	*Picea abies*
Pinus misc	*Pinus cembra*; *Pinus mugo arborea*; *Pinus nigra* *Pinus nigra subsp. laricio*
Pinus pinaster	*Pinus pinaster*
Pinus sylvestris	*Pinus sylvestris*
Pseudotsuga menziesii	*Pseudotsuga menziesii*
Quercus misc	*Quercus cerris*; *Quercus frainetto*; *Quercus ilex*; *Quercus pubescens*
Quercus robur & Quercus petraea	*Quercus robur*; *Quercus petraea*

Table S3. Overview of all combinations of Global Climate Models (GCMs) – Regional Climate Models (RCMs) and ensemble members used for downloading simulated data of 2m air temperature and 2m relative humidity from the Copernicus Climate Data Store in the framework of the Coordinated Regional Climate Downscaling Experiment (CORDEX) for the two climate scenarios of Representative Concentration Pathways (RCPs) 4.5 and 8.5. RCM data on a high regional resolution (here: European domain; 0.11° x 0.11°) depend on output from GCMs for lateral and lower boundary conditions. Temporal resolution of downloaded data was 3 hours and time period was 2068-2082.

Climate scenario	GCM	RCM	ensemble member
RCP 4.5	CNRM-CERFACS-CM5	KNMI-RACMO22E	r1i1p1
	ICHEC-EC-EARTH	DMI-HIRHAM5	r3i1p1
	ICHEC-EC-EARTH	GERICS-REMO2015	r12i1p1
	ICHEC-EC-EARTH	KNMI-RACMO22E	r1i1p1
	ICHEC-EC-EARTH	SMHI-RC4A	r12i1p1
	IPSL-CM5A-MR	SMHI-RC4A	r1i1p1
	MOHC-HadGEM2-ES	GERICS-REMO2015	r1i1p1
	MOHC-HadGEM2-ES	KNMI-RACMO22E	r1i1p1
	MOHC-HadGEM2-ES	SMHI-RC4A	r1i1p1
	MPI-M-MPI-ESM-LR	SMHI-RC4A	r1i1p1
	NCC-NorESM1-M	DMI-HIRHAM5	r1i1p1
	NCC-NorESM1-M	GERICS-REMO2015	r1i1p1
	NCC-NorESM1-M	SMHI-RC4A	r1i1p1
RCP 8.5	CCCma-CanESM2	CLMcom-CLM-CCLM4-8-17	r1i1p1
	CNRM-CERFACS-CM5	CLMcom-ETH-COSMO-crCLIM	r1i1p1
	CNRM-CERFACS-CM5	GERICS-REMO2015	r1i1p1
	ICHEC-EC-EARTH	CLMcom-ETH-COSMO-crCLIM	r12i1p1
	ICHEC-EC-EARTH	KNMI-RACMO22E	r12i1p1
	ICHEC-EC-EARTH	SMHI-RCA4	r12i1p1
	IPSL-CM5A-MR	DMI-HIRHAM5	r1i1p1
	MIROC-MIROC5	CLMcom-CLM-CCLM4-8-17	r1i1p1
	MOHC-HadGEM2-ES	SMHI-RCA4	r1i1p1
	MPI-M-MPI-ESM-LR	DMI-HIRHAM5	r1i1p1
	NCC-NorESM1-M	CLMcom-ETH-COSMO-crCLIM	r1i1p1
	NCC-NorESM1-M	GERICS-REMO2015	r1i1p1
	NCC-NorESM1-M	KNMI-RACMO22E	r1i1p1

Table S4. Overview of relative uncertainty values for different parameters per forest tree species group propagated by error propagation principle for every spatial tile of the forest foliar Hg uptake flux map (Fig. 1).

Tree species group[a]	relative uncertainty (ru)						
	LMA[b]	DMA[c]	LAI[d]	Forest area[e]	cf_{age} [f]	pine[g]	**total**[h]
Abies spp	0.36				0.03	-	0.70
Betula spp	0.61				-	-	0.86
Broadleaved mixed	0.82				-	-	1.02
Carpinus spp	0.18				-	-	0.63
Fagus spp	0.47				-	-	0.77
Fraxinus spp	0.54	0.1	0.44	0.40	-	-	0.81
Larix spp	0.76				-	-	0.97
Picea spp	0.75				0.03	-	0.96
Pine	0.72				0.06	0.014	0.94
Pseudotsuga menziesii	0.69				0.06	-	0.92
Quercus misc	0.28				-	-	0.67
Quercus robur & Quercus petraea	0.52				-	-	0.80

a See Table S2 for an overview of tree species aggregated into tree species groups. For the group of mixed conifer species (Table S2), we calculated an average uncertainty value from total uncertainty values of coniferous needle tree species groups, which equals 0.90.

b Leaf mass per area (LMA) values per tree species group were obtained from Forrester et al., 2017. The relative uncertainty of LMA per tree species group was calculated including the range of all LMA values within each respective tree species group: (maximum LMA - minimum LMA)/(average LMA).

c Foliar Hg values were obtained from a dataset of Hg concentrations in foliage samples of the ICP Forests biomonitoring network and the Austrian Bio-Indicator Grid measured using a direct mercury analyzer (DMA) (see Sect. **??** and Wohlgemuth et al., 2022). A DMA measurement sequence of foliar Hg concentrations was accepted when primary liquid reference standards did not deviate by more than ± 10% from target value.

d Relative root mean square deviation (RMSD) of the leaf area index (LAI) product from PROBA-V from LAI ground observations evaluated by Fuster et al. (2020).

e The uncertainty of the proportion of tree species per forest land area (spatial resolution: 1 km^2) was not evaluated by Brus et al., 2012 and depends on the heterogenous availability of national forest inventories in Europe. From the overall accuracy given in Brus et al., 2012, we estimated a relative uncertainty value of 0.4 per tree species and km^2.

f Uncertainty of the correction factor (cf_{age}) for upscaling Hg uptake rates of needles of different age classes to whole coniferous evergreen trees (see Wohlgemuth et al., 2020).

g Relative RMSD of the linear regression slope of the average daily pine needle Hg uptake rate vs. time proportion of VPD > 1.2 kPa (see Wohlgemuth et al., 2022).

h Total species uncertainty $= \sqrt{ru^2_{LMA} + ru^2_{DMA} + ru^2_{LAI} + ru^2_{for.area} + ru^2_{cfage} + ru^2_{pine}}$